Biomedicine & Pharmacotherapy 168 (2023) 115745

Contents lists available at ScienceDirect

Biomedicine & Pharmacotherapy

journal homepage: www.elsevier.com/locate/biopha

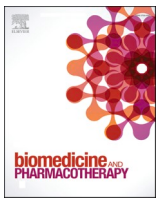

The 3-(3-oxoisoindolin-1-yl)pentane-2,4-dione (ISOAC1) as a new molecule able to inhibit Amyloid β aggregation and neurotoxicity

Ilaria Piccialli [a], Francesca Greco [b], Giovanni Roviello [c], Maria Josè Sisalli [a], Valentina Tedeschi [a], Antonia di Mola [d], Nicola Borbone [b], Giorgia Oliviero [e], Vincenzo De Feo [f], Agnese Secondo [a], Antonio Massa [d,*], Anna Pannaccione [a,*]

[a] Division of Pharmacology, Department of Neuroscience, Reproductive and Dentistry Sciences, School of Medicine, Federico II University of Naples, Naples, Italy
[b] Department of Pharmacy, Federico II University of Naples, Naples, Italy
[c] Institute of Biostructures and Bioimaging, Italian National Council for Research (IBB-CNR), Naples, Italy
[d] Department of Chemistry and Biology "A. Zambelli", University of Salerno, Fisciano, SA, Italy
[e] Department of Molecular Medicine and Medical Biotechnologies, Federico II University of Naples, Naples, Italy
[f] Department of Pharmacy, University of Salerno, Fisciano, SA, Italy

ARTICLE INFO

Keywords:
β-diketone-3-substituted isoindolinone
Amyloid β 1–42 aggregation
Alzheimer's disease
Neuroprotection

ABSTRACT

Amyloid β 1–42 ($A\beta_{1-42}$) protein aggregation is considered one of the main triggers of Alzheimer's disease (AD). In this study, we examined the *in vitro* anti-amyloidogenic activity of the isoindolinone derivative 3-(3-oxoisoindolin-1-yl)pentane-2,4-dione (ISOAC1) and its neuroprotective potential against the $A\beta_{1-42}$ toxicity. By performing the Thioflavin T fluorescence assay, Western blotting analyses, and Circular Dichroism experiments, we found that ISOAC1 was able to reduce the $A\beta_{1-42}$ aggregation and conformational transition towards β-sheet structures. Interestingly, *in silico* studies revealed that ISOAC1 was able to bind to both the monomer and a pentameric protofibril of $A\beta_{1-42}$, establishing a hydrophobic interaction with the PHE19 residue of the $A\beta_{1-42}$ KLVFF motif. *In vitro* analyses on primary cortical neurons showed that ISOAC1 counteracted the increase of intracellular Ca^{2+} levels and decreased the $A\beta_{1-42}$-induced toxicity, in terms of mitochondrial activity reduction and increase of reactive oxygen species production. In addition, confocal microscopy analyses showed that ISOAC1 was able to reduce the $A\beta_{1-42}$ intraneuronal accumulation. Collectively, our results clearly show that ISOAC1 exerts a neuroprotective effect by reducing the $A\beta_{1-42}$ aggregation and toxicity, hence emerging as a promising compound for the development of new Aβ-targeting therapeutic strategies for AD treatment.

1. Introduction

Alzheimer's disease (AD) is one of the most common neurodegenerative disorders and accounts for 70% of all dementia cases worldwide. The patients diagnosed with AD are affected by a progressive deterioration of cognitive abilities and are characterized, at the brain level, by the presence of large extracellular deposits of aggregated Amyloid β (Aβ) peptides, along with degenerating neurons containing neurofibrillary tangles [1,2]. The Aβ aggregates, whose accumulation starts many years before AD is clinically diagnosed [3], have been extensively studied in the last decades, since they are considered the main molecular factor causing the AD syndrome [4]. Indeed, according to the "amyloid cascade hypothesis", the Aβ aggregates exert their toxicity in different cell types affecting a myriad of cellular functions, ultimately resulting in neurodegeneration and neuroinflammation [5,6].

The Aβ peptide, consisting of 39–43 amino acid residues, is generated upon the cleavage of the amyloid precursor protein (APP) [7], a large transmembrane protein involved in many neuronal physiological functions [8]. The Aβ aggregation is a multistep process that passes through different intermediates including low molecular weight (LMW) and high molecular weight (HMW) oligomers, protofibrils and finally fibrils, which are polypeptide aggregates with a core structure of parallel β-sheets [9]. Among all the Aβ species, the prefibrillar intermediates such as soluble oligomers and protofibrils are more potent than Aβ fibrils, and are responsible for synaptic degeneration and neuronal dysfunction and death in the pre-clinical stage of AD [10–12]. Many drugs have been developed thus far targeting β- and γ-secretases, the two principal enzymes responsible for the Aβ production [13,14], but they

* Corresponding authors.
E-mail addresses: amassa@unisa.it (A. Massa), pannacio@unina.it (A. Pannaccione).

https://doi.org/10.1016/j.biopha.2023.115745
Received 23 August 2023; Received in revised form 12 October 2023; Accepted 16 October 2023
Available online 21 October 2023

produced undesirable results in clinical trials due to the lack of specificity or the presence of serious side effects and toxicity [15]. Therefore, directly targeting the Aβ aggregation process could still represent a route to explore in the search of therapeutic strategies to prevent or treat AD.

Based on this hypothesis, several molecules such as polyphenols [16], antibodies [17], and peptides [18] have been tested for their ability to inhibit the Aβ aggregation at its early stages. Several peptides, called "β-sheet-breakers" have been conceived to suppress amyloid aggregation by interfering with the formation of β-sheet structures [18], which is not only a crucial step of fibrillogenesis but also the key structural feature conferring neurotoxicity to the prefibrillar Aβ intermediates [19,20]. Many of these molecules are capable to recognize the hydrophobic core ^{16}KLVFFA^{21} of Aβ, which plays a crucial role in the formation of β-sheet structures and aggregation [21–24].

Many difficulties in designing new anti-aggregating compounds suitable for the treatment of AD arise from the strict requirements needed for their clinical use, including low molecular weight, the adequate lipophilicity necessary to cross cell membranes and the blood brain barrier, and minimal toxicity. In this context, hybrid small molecules may be of great interest for their easy accessibility. Moreover, considered that multi-target approaches are among the most promising strategies to treat AD due to the complex nature of the disease, molecules capable of targeting simultaneously multiple pathogenic mechanisms deserve to be tested for their neuroprotective potential [25]. Recently, our group reported a library of small molecules containing an isoindolinone ring as heterocycle pharmacophore [26–28]. Among them, we selected the 3-(3-oxoisoindolin-1-yl)pentane-2,4-dione (ISOAC1), possessing the isoindolinone ring linked to a β-diketone group exhibiting keto-enol tautomerism and metal binding properties towards Cu(II), Fe(II), and Al(III) [26]. Notably, the isoindolinone analogue of Donepezil has been reported to exhibit an inhibitory activity on Aβ aggregation, in addition to an anti-AchE activity comparable to that of Donepezil [29,30]. Similarly, other isoindoline-1,3-dione derivatives were reported to act as cholinesterase and Aβ aggregation inhibitors [31]. In the present study, we evaluated the possible inhibitory effect of ISOAC1 on the $A\beta_{1-42}$ self-aggregation by using multiple techniques, and performed *in silico* studies to investigate the ISOAC1-$A\beta_{1-42}$ interaction. Moreover, we examined the ability of ISOAC1 to protect primary cortical neurons from the multifaceted $A\beta_{1-42}$ toxicity.

2. Materials and methods

All the animal procedures were conducted with the approval of the Ethics Committee of the Federico II University of Naples, in accordance with the regulation 2010/63 from EU, the D.Lgs. 2014/26 from Italian Ministry of Health.

2.1. ISOAC1 molecule preparation

The molecule 3-(3-oxoisoindolin-1-yl)pentane-2,4-dione was synthesized as previously described [26,27]. The molecule was dissolved in dimethyl sulfoxide (DMSO, Sigma-Aldrich, Milan, Italy) to a final concentration of 10 mM, and aliquots were stored at −20 °C until use.

2.2. Peptide solubilization and preparation of $A\beta_{1-42}$ solutions

The chemical construct of the Aβ peptide was synthesized by the custom peptide service of GenicBio (Shanghai, China) using the $A\beta_{1-42}$ sequence of human APP. The peptides were 95% pure as revealed by high performance liquid chromatography and mass spectrometry. Prior to resuspension, lyophilized $A\beta_{1-42}$ was solubilized in 1,1,1,3,3,3-hexafluoro-2-propanol (HFIP; Sigma-Aldrich, Milan, Italy) to 1 mM as previously reported [32,33], and sonicated in an ice bath to eliminate any preformed peptide assemblies [34]. The clear solution containing the dissolved peptide was then aliquoted in microcentrifuge tubes and dried under vacuum in a SpeedVac until complete elimination of the solvent. The resulting film was stored at −80 °C. HFIP is largely used to obtain a fully monomeric state of peptides before starting aggregation experiments. Moreover, the stage of Aβ dissolution in HFIP is included in a standardized protocol to prepare aggregate-free Aβ samples for biophysical and biological studies of AD [35]. To prepare the fresh $A\beta_{1-42}$ monomer solutions, each $A\beta_{1-42}$ aliquot was allowed to equilibrate to room temperature, carefully resuspended in 10 mM NaOH to a concentration of 5 mM, and then diluted in 10 mM (4-(2-hydroxyethyl)−1-piperazineethanesulfonic acid (HEPES; Sigma-Aldrich, Milan, Italy), pH 7.4, to different final concentrations immediately prior to use, as previously described [22]. For Thioflavin T (ThT) assay and Western blotting, $A\beta_{1-42}$ was incubated at the final concentration of 50 μM alone or with ISOAC1 at different molar ratios in 10 mM HEPES (pH 7.4) at 37 °C for 4 days with continuously shacking. To treat cells, 50 μM of pre-aggregated or freshly reconstituted $A\beta_{1-42}$ were diluted in culture medium at the desired final concentrations.

2.3. Thioflavin T fluorescence assay

ThT fluorescence assay, used to detect β-sheet aggregates of the $A\beta_{1-42}$ peptide, was performed by an EnSpire Multimode Plate Reader (PerkinElmer). Briefly, after 96 h of incubation the samples containing 50 μM $A\beta_{1-42}$ with or without ISOAC1 were diluted 1:10 with 50 mM glycine-NaOH buffer (pH 8.0) containing ThT (50 μM; Sigma-Aldrich, Milan, Italy) to a final volume of 200 μL. We selected 50 μM as the final ThT concentration since it was shown to be the most suitable concentration to perform end-point analyses on pre-aggregated $A\beta_{1-42}$ [36]. The fluorescent intensity of each sample was recorded (excitation wavelength, 440 nm; emission wavelength, 485 nm). Blanks using HEPES (pH 7.4) instead of the mixtures of $A\beta_{1-42}$ with or without ISOAC1 were also carried out. Since ThT becomes self-fluorescent at concentrations above 5 μM [36], we measured the fluorescence of 50 μM ThT alone and the fluorescence intensity of the protein samples was corrected for the background ThT signal.

2.4. Western blotting

Gel electrophoresis and Western blotting analyses were performed on pre-aggregated $A\beta_{1-42}$ preparations. Briefly, after determination of protein concentration, unheated samples were diluted in 1X Laemmli buffer with 5% β-mercaptoethanol and electrophoresed on 4–20% Tris-Glycine polyacrylamide gels (Bio-Rad Laboratories, Milan, Italy) in sodium dodecyl sulfate running buffer. After electrophoresis, gels were blotted onto 0.45-μm polyvinylidene difluoride membranes (Millipore, Darmstad, Germany) overnight. Post-transfer membranes were blocked in 5% bovine serum albumin (BSA; Cell signaling, Massachusetts, USA) in Tris-buffered saline containing 0.1% Tween 20 and then incubated with the anti-$A\beta_{1-42}$ (D54D2) rabbit monoclonal antibody (1:1000 in BSA; Cell Signaling, Massachusetts, USA, #8243), which recognizes an epitope within residues 17–42 of human Aβ. Immunoreactivity was detected using enhanced chemiluminescence (ECL; Amersham Biosciences) and the films were developed with a standard photographic procedure.

Western blotting analysis on SH-SY5Y cell lysates were performed as previously described [53]. Post-transfer membranes were incubated with the anti-cytochrome C rabbit polyclonal antibody (1:1000 in BSA; Cell Signaling, Massachusetts, USA, #4272 S).

2.5. Circular dichroism measurements

The $A\beta_{1-42}$ samples for the circular dichroism (CD) experiments were used on their disaggregated state. As described elsewhere [37], the aggregate-free $A\beta_{1-42}$, stored at −20 °C as a dry sample, was dissolved in 20 mM NaOH solution to a final concentration of 0.5 mM. The solution was sonicated for one minute and then allowed to equilibrate to room temperature for 5 min. Then, the 0.5 mM peptide solution was

centrifuged for 20 min at 13 000 rpm at 25 °C just before CD acquisition. The supernatant was collected and resuspended in 10 mM K^+ buffer (9 mM KCl and 1 mM KH_2PO_4), pH 7.4, to be analyzed at approximately 20 μM final concentration. For the samples containing ISOAC1 at 1.25, 2.5, and 5 equivalents, the 20 μM aggregate-free $A\beta_{1-42}$ solution was prepared as mentioned above and the compound was added just before the CD analysis. CD spectra were acquired on a Jasco 1500 spectropolarimeter equipped with a Jasco PTC-348-WI temperature controller (Jasco Europe S.r.l, Milan, Italy). The CD spectra were recorded using a 0.1 cm path length cuvette and each acquisition was averaged over three scans at 37 °C with a scan rate of 200 nm min^{-1}, response time of 4 s, bandwidth of 2 nm. The contribution of the buffer was subtracted from each spectrum. Each spectrum was recorded at 24-hour-time point and the samples were kept at 37 °C to maintain the fibrillation conditions between measurements.

2.6. In silico studies

The three-dimensional structures of the $A\beta_{1-42}$ monomer (PDB ID: 1IYT) and the pentameric protofibril model (PDB ID: 2BEG) were obtained from Protein Data Bank [38]. The 2D structure for ISOAC1 was drawn using the molecular editor provided in 1-Click Mcule (Mcule Inc., Palo Alto, CA, USA) [39, 40–42], a web-based platform powered by AutoDockVina docking algorithm [43], by which we realized our docking experiments. The atomic coordinates of the binding site were: X = −0.619, Y = 0.557, and Z = 9.143 [44], and the size of the binding site was 22 Å. We selected the docking poses with the most negative docking scores (kcal/mol) corresponding to the highest binding affinities. The molecular graphics program incorporated in 1-Clik Mcule was used for structural visualization of peptide-ligand interactions and to obtain the snapshots of Figs. 3**B**, 3**C**, and 3**E**, while H-bondings were analyzed by WebLabViewerPro (Molecular Simulations Inc., San Diego, CA, USA). The peptide-ligand interaction diagrams reported in Figs. 3**D and** 3**F** were obtained by ProteinsPlus (https://proteins.plus/, accessed on June 19, 2023).

2.7. Cell cultures

Human SH-SY5Y cells were grown as monolayers in a Dulbecco's modified Eagle's medium (DMEM) supplemented with 10% FBS, 1% penicillin (50 IU/mL), and streptomycin (50 μg/mL) in a humidified atmosphere at 37 °C with 5% CO_2. The cells were neuronally differentiated with retinoic acid (10μM, 48h). Rat primary cortical neurons were obtained from the brains of 14/16-day-old Wistar rat embryos, dissected and cultured as previously reported [45–47].

2.8. MTT assay

Mitochondrial activity was assessed by the MTT (3[4,5-dimethylthiazol-2-yl]−2,5-diphenyl-tetrazolium bromide) assay, as previously reported [48]. Briefly, after treatments, neurons were incubated with a MTT solution (1 h at 37 °C). In viable cells, the mitochondrial dehydrogenases convert the MTT reagent into water-insoluble formazan crystals. At the end of the incubation, insoluble crystals were dissolved in DMSO and the absorbance was determined spectrophotometrically at 540 nm. The data are expressed as a percentage of mitochondrial activity relative to control values.

2.9. Measurement of reactive oxygen species

Measurement of intracellular reactive oxygen species (ROS) levels was performed as previously described [49]. Briefly, the cortical neurons were seeded on glass coverslips and exposed to $A\beta_{1-42}$ preparations. At the end of each treatment the neurons were pre-loaded with 2′, 7′-dichlorofluorescein diacetate (DCFH-DA, 10 μM) for 30 min at 37 °C in the dark. Cells were washed with PBS and the reaction was stopped by adding 2,6-di-tert-butyl-4-methylphenol (0.2% in ethanol) and ethylenediaminetetraacetic acid (EDTA, 2 mM). Fluorescence intensity was then analyzed with an Axiovert200 microscope (Carl Zeiss, Milan, Italy) connected to the MicroMax 512BFT cooled CCD camera (Princeton Instruments, USA), LAMBDA10–2 filter wheeler (Sutter Instruments, Novato, California, USA), and Meta-Morph/MetaFluor Imaging System software (Universal Imaging, Bedford Hills, New York, USA). Each coverslip was exposed to 485 nm excitation wavelenght for 10 seconds and the emitted light was passed through a 530 nm barrier filter.

2.10. $[Ca^{2+}]_i$ measurements

Intracellular Ca^{2+} concentrations ($[Ca^{2+}]_i$) were measured in primary cortical neurons by single-cell computer-assisted video imaging as previously reported [50]. Fura-2 experiments were carried out with the Axiovert200 microscope (Carl Zeiss, Milan, Italy) connected to the MicroMax 512BFT cooled CCD camera (Princeton Instruments, USA), LAMBDA10–2 filter wheeler (Sutter Instruments, Novato, California, USA), and Meta-Morph/MetaFluor Imaging System software (Universal Imaging, Bedford Hills, New York, USA). Neurons were alternatively illuminated at wavelengths of 340 and 380 nm by a Xenon lamp and the emitted light was passed through a 512 nm barrier filter. Fluorescence intensity was measured every 3 s and $[Ca^{2+}]_i$ was calculated by the equation of Grynkiewicz et al. [51,52].

2.11. Confocal microscopy

The mitochondrial membrane potential (ΔΨm) and Fluo-3 cytosolic $[Ca^{2+}]$ measurements were performed as previously described [53,54]. Briefly, the neuronally differentiated SH-SY5Y cells were loaded with the Fluo-3AM acetoxymethil ester (5 nM) and thetetramethylrhodamine ethyl ester (TMRE; 20 nM) for 30 min in a medium containing: 156 mM NaCl, 3 mM KCl, 2 mM $MgSO_4$, 1.25 mM KH_2PO_4, 2 mM $CaCl_2$, 10 mM glucose, and 10 mM HEPES (pH adjusted to 7.35 with NaOH). At the end of the incubation, cells were washed 3 times in the same medium. An increase in $[Ca^{2+}]$ intensity of fluorescence was indicative of cytosolic Ca^{2+} overload [48], while a decline in the mitochondria-localized intensity of TMRE fluorescence was indicative of mitochondrial membrane depolarization [55]. The illumination intensity of 543 Xenon laser used to excite TMRE, and of 488 Argon laser used to excite Fluo-3AM fluorescence, was kept to a minimum of 0.5% of laser output to avoid phototoxicity.

For immunocytochemical analyses, rat primary cortical neurons were cultured on glass coverslips. After 8 days in culture, neurons were subjected to the selected treatments for 24 h. At the end of the treatments, the neurons were washed twice in 0.01 M cold PBS at pH 7.4 and fixed in 4% (w/v) paraformaldehyde for 20 min at room temperature. After three washes in PBS, neurons were blocked in PBS containing 3% (w/v) BSA for 30 min and then incubated overnight at 4 °C with the rabbit monoclonal anti-$A\beta_{1-42}$ antibody (1:1000; Cell signaling, Massachusetts, USA). The control for the specificity of the antibody against $A\beta_{1-42}$ was performed with its replacement with normal serum as previously described [56]. Then, neurons were washed with PBS and incubated with anti-rabbit Cy3-conjugated antibody (1:200; Jackson Immuno Research Laboratories, Inc., West Grove, PA, USA) for 1 h at room temperature under dark conditions. Glass coverslips were mounted with a SlowFade Antifade Kit (Molecular Probes, Life Technologies, Milan, Italy) and acquired by a 63 × oil immersion objective using a Zeiss inverted700 confocal microscope.

2.12. Statistics

GraphPad Prism 6.02 was used for statistical analyses (GraphPad Software, La Jolla, CA). The data are expressed as mean ± S.E.M. of the values obtained from individual experiments. Statistical comparisons between groups were performed by one-way analysis of variance

(ANOVA) followed by Bonferroni *post hoc* test or Newman-Keuls' test; $p < 0.05$ was considered significant.

3. Results and discussion

3.1. The β-diketone-3-substituted isoindolinone ISOAC1 reduces the formation of $A\beta_{1-42}$ aggregates and prevents their toxicity in neuronally-differentiated SH-SY5Y cells

In consideration of the anti-aggregating potential of some isoindolinone derivatives reported in literature [29–31], we explored the anti-aggregating properties of the β-diketone-3-substituted isoindolinone ISOAC1. Although the Aβ aggregation may result from several mechanisms and different molecular factors including metal ions have been found to influence the aggregation process [57], we decided to examine the ISOAC1 inhibitory activity against the self-induced Aβ aggregation, as this remains the most appropriate test to detect any direct anti-aggregating activity of candidate inhibitors [35]. The $A\beta_{1-42}$ peptide was preferred, since it is the main responsible of the amyloid burden in AD brains [4]. We first performed end-point ThT experiments, a commonly used method to quantify pre-formed amyloid aggregates [58]. In this fluorometric assay, the benzothiazole dye, ThT, interacts with the cross β-sheet quaternary structure of the amyloid protein and emits a strong fluorescence signal at approximately 482 nm when

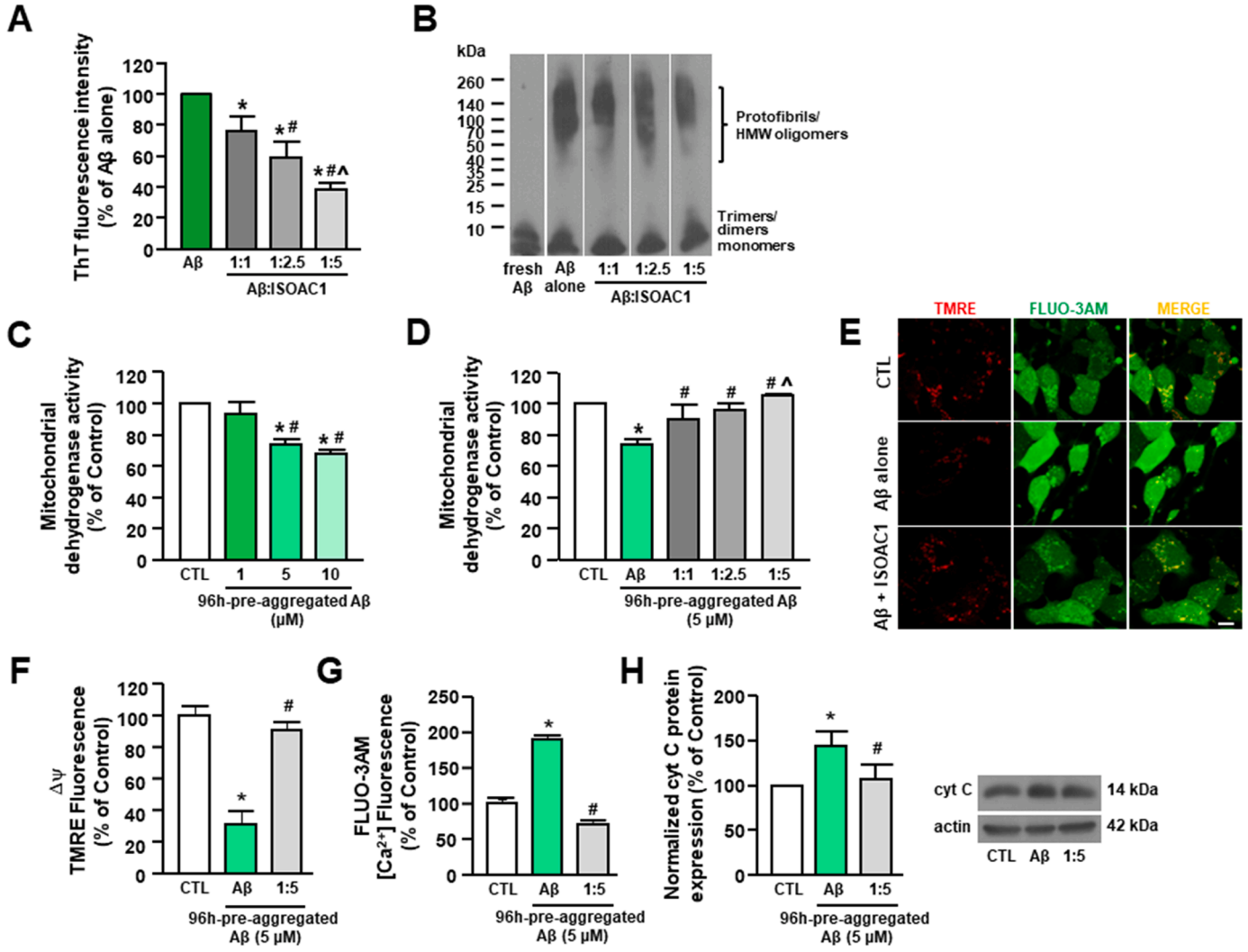

Fig. 1. The co-incubation with ISOAC1 reduces the formation of $A\beta_{1-42}$ aggregates and their toxicity at the mitochondrial level in neuronally-differentiated SH-SY5Y cells. ThT fluorescence intensity of $A\beta_{1-42}$ measured after 96 h of incubation at 37 °C in the absence and in the presence of different molar excesses of ISOAC1 and represented as percentage of $A\beta_{1-42}$ alone. Data are expressed as mean ± S.E.M. of 3 independent experimental sessions. * $p < 0.05$ *vs* $A\beta_{1-42}$ alone; # $p < 0.05$ *vs* 1:1; ^ $p < 0.05$ *vs* 1:2.5. Representative Western blotting of $A\beta_{1-42}$ incubated at 37 °C for 96 h in the absence and in the presence of different molar excesses of ISOAC1, separated by gel electrophoresis on a 4–20% Tris-glycine polyacrylamide gel, probed with the monoclonal antibody D54D2, and visualized by enhanced chemiluminescence (B). Evaluation of mitochondrial dehydrogenase activity in differentiated SH-SY5Y cells treated with $A\beta_{1-42}$ pre-aggregated for 96 h at 1, 5, 10 μM (final concentrations in the culture medium). Data are expressed as mean ± S.E.M. of 3 independent experimental sessions. * $p < 0.05$ *vs* Control; # $p < 0.05$ *vs* 1 μM (C). Evaluation of mitochondrial dehydrogenase activity in differentiated SH-SY5Y cells treated with 5 μM $A\beta_{1-42}$ pre-aggregated alone or in the presence of different molar excesses of ISOAC1. Data are expressed as mean ± S.E.M. of 3 independent experimental sessions. * $p < 0.05$ *vs* Control; # $p < 0.05$ *vs* $A\beta_{1-42}$alone; ^ $p < 0.05$ *vs* 1:1 (D). Quantification of mitochondrial membrane potential and cytosolic [Ca^{2+}] in untreated SH-SY5Y cells and in cells treated with 5 μM $A\beta_{1-42}$ pre-aggregated alone or in the presence of ISOAC1 at 1:5 Aβ:ISOAC1 molar ratio (E-G). Data are expressed as mean ± S.E.M. of 3 independent experimental sessions ($n = 40$ cells for each group of three experimental sessions) * $p < 0.05$ *vs* Control; # $p < 0.05$ *vs* $A\beta_{1-42}$ alone. Representative Western blotting (right) and densitometric quantification (left) of cytochrome C protein expression in untreated SH-SY5Y cells and in cells treated with 5 μM $A\beta_{1-42}$ pre-aggregated alone or in the presence of ISOAC1 at 1:5 Aβ:ISOAC1 molar ratio (H). Data are expressed as mean ± S.E.M. of 3 independent experimental sessions * $p < 0.05$ *vs* Control; # $p < 0.05$ *vs* $A\beta_{1-42}$ alone.

excited at 440–450 nm. Importantly, it was found that the ThT fluorescence intensity linearly correlates with the amyloid aggregates concentration [36,59], as the amyloid species resulting from the aggregation process are mainly composed of aggregates with a β-sheet conformation [60,61]. The assay was performed after incubating the freshly dissolved $A\beta_{1-42}$ peptide for 96 h at 37 °C with continuous shacking, a set of conditions that was shown to induce aggregation [62–64], both in the absence and in the presence of ISOAC1 at different Aβ:ISOAC1 molar ratios (1:1.25, 1:2.5, and 1:5). Interestingly, the obtained results showed that ISOAC1 was able to significantly reduce the content of β-sheet aggregates in a concentration-dependent manner (Fig. 1**A**), with the maximum reduction at the 1:5 Aβ:ISOAC1 molar ratio.

To assess any changes in the amount and/or in the size of the $A\beta_{1-42}$ aggregates formed in the presence of ISOAC1, Western blotting analyses have also been performed. In particular, 2 μg from 50 μM freshly prepared $A\beta_{1-42}$ and from the same samples used for the ThT assay were loaded onto 4–12% polyacrylamide gels. The membranes were blotted with an anti-$A\beta_{1-42}$ antibody recognizing an epitope within residues 17–42 of human Aβ, able to detect the monomer, and both small and large $A\beta_{1-42}$ aggregates, including amyloid plaques [32,65]. In accordance with previous reports, the freshly prepared $A\beta_{1-42}$ immediately added to the gel ran mostly as monomer, even if low-n oligomeric species (dimers and trimers) were already present [66,67]. After aggregation under fibril-forming conditions, the $A\beta_{1-42}$ samples produced a typical migration pattern in which monomer and dimer/trimer bands, although not well resolved, were clearly detectable, while HMW oligomers produced a smeared signal above 40 kDa (Fig. 1**B**) [34,67,68]. Importantly, the co-incubation with ISOAC1 caused a reduction in the signal intensity of the smear above 40 kDa, likely reflecting a decrease in the content of HMW species (Fig. 1**B**). In particular, the densitometric quantification revealed that the Aβ aggregates ranging between 35 and 60 kDa were significantly reduced only at the 1:5 Aβ:ISOAC1 molar ratio in comparison to the Aβ sample incubated alone (Mean diff. −50.80%) (Fig. S1A). The Aβ aggregates ranging between 60 and 100 kDa were significantly reduced at all the Aβ:ISOAC1 tested ratios in comparison to Aβ alone (Mean diff. −29.79 at 1:1.25, −34.65 at 1:2.5, −29.15 at 1:5 molar ratios) (Fig. S1B). By contrast, no significant difference was found between the Aβ sample incubated alone and those incubated with ISOAC1 at any of the tested molar ratios (Fig. S1C).

Taken together, both the ThT and Western blotting experiments provided evidence that ISOAC1 was able to interfere with the $A\beta_{1-42}$ aggregation process, ultimately resulting in the reduction of β-sheet aggregates. Given the critical role attributed to HMW oligomers and protofibrils, and to the β-sheet conformation as crucial structural feature conferring neurotoxicity to different Aβ species, we investigated the toxicity of $A\beta_{1-42}$ aggregates grown in the presence and in the absence of ISOAC1 in SH-SY5Y neuroblastoma cells, differentiated through a well-established protocol [69]. At first, we performed concentration-response experiments by exposing differentiated SH-SY5Y cells to 1, 5, and 10 μM $A\beta_{1-42}$ previously incubated for 96 h to induce aggregation. Cells were treated for 24 h prior to assess the cell metabolic activity reduction, which is a well-established marker of early mitochondrial toxicity. Of note, the MTT assay did not show any significant reduction of the mitochondrial dehydrogenase activity in SH-SY5Y cells exposed to 1 μM $A\beta_{1-42}$ in comparison to the untreated cells (Fig. 1**C**). By contrast, both 5 and 10 μM $A\beta_{1-42}$ were able to significantly reduce mitochondrial metabolism in comparison to the untreated cells and to the cells treated with 1 μM $A\beta_{1-42}$, even if no significant difference was found between these two concentrations (Fig. 1**C**). Then, we evaluated the mitochondrial dehydrogenase activity of the SH-SY5Y cells exposed for 24 h to 5 μM $A\beta_{1-42}$ samples pre-aggregated in the presence of ISOAC1 at 1:1.25, 1:2.5, and 1:5 Aβ:ISOAC1 molar ratios. As shown in Fig. 1**D**, the $A\beta_{1-42}$ aggregates grown in the presence of ISOAC1 did not produce any significant reduction of mitochondrial dehydrogenase activity in comparison to that observed in the untreated cells, while resulting significantly less toxic if compared to the $A\beta_{1-42}$ aggregates grown alone (Fig. 1**D**).

To further investigate the cellular toxicity, particularly at the mitochondrial level, exerted by the pre-aggregated $A\beta_{1-42}$, we performed confocal microscopy experiments using the fluorescent probes Fluo-3 and TMRE to measure the cytosolic Ca^{2+} levels and ΔΨm, respectively. As for the MTT assay, differentiated SH-SY5Y cells were exposed for 24 h to 5 μM $A\beta_{1-42}$ pre-aggregated both alone and in the presence of ISOAC1 (1:5 Aβ:ISOAC1 molar ratio). Interestingly, we found that the $A\beta_{1-42}$ pre-aggregated alone induced the depolarization of mitochondrial membrane and the increase of cytosolic Ca^{2+} levels (Fig. 1**E-G**). In addition, we found that the mitochondrial membrane depolarization was accompanied by the release of cytochrome C, a marker of mitochondrial damage (Fig. 1**H**). Of note, $A\beta_{1-42}$ aggregates grown in the presence of ISOAC1 (1:5) failed to induce these alterations (Fig. 1**E-H**), therefore displaying no toxicity in comparison to $A\beta_{1-42}$ pre-aggregated alone.

Notably, the loss of toxicity of the Aβ aggregates grown in the presence of ISOAC1 at the 1:5 molar ratio correlated with the reduction in the Aβ species ranging between 35 and 60 kDa, (Fig. 1**B** and Fig. S1A), likely comprising Aβ dodecamers/Aβ* 56. In agreement, previous studies reported that Aβ dodecamers were able to increase intracellular Ca^{2+} levels in neurons by interacting with the N-methyl-D-aspartate (NMDA) receptors [70], and to disrupt neuronal membrane to a greater extent than mature Aβ fibrils [71]. Of note, they were also found to be the main responsible for the cell damage induced by an oligomeric Aβ mixture, as their removal completely resulted in the loss of toxicity [72]. Therefore, it is possible to hypothesize that ISOAC1, interfering with the Aβ aggregation, prevented the formation of specific, toxic Aβ species.

3.2. The β-diketone-3-substituted isoindolinone ISOAC1 inhibits the conformational transition of $A\beta_{1-42}$ to β-sheet structures

It is well known that the conformational transition of the Aβ protein from an unordered secondary structure to a β-sheet structure is the crucial step of fibrillogenesis [73] and that, conversely, after fibril formation Aβ peptides attained predominately a β-sheet conformation [60,61]. Therefore, we performed CD spectroscopy analyses in the range of 190–260 nm in order to investigate whether ISOAC1 was able to affect the conformational transition of the $A\beta_{1-42}$ peptide to β-sheet structures. First, we conducted a time-course experiment to analyze the conformational transition of pure $A\beta_{1-42}$ samples in a time-frame of 96 h. The CD experiments showed that the $A\beta_{1-42}$ peptide underwent a progressive change in the secondary structure and that, after 96 h, it was chiefly composed of β-sheet structures (Fig. 2**A**). More specifically, the freshly prepared $A\beta_{1-42}$ sample exhibited a major negative peak below 200 nm, which is typical of a random-coil conformation, to gradually undergoing a transition toward the β-sheet pattern as the incubation time proceeded. In particular, the appearance of a negative peak around 220 nm along with a positive peak at 195–200 nm, weakly visible at 48 h and more pronounced at 72 and 96 h, clearly indicated the presence of β-sheet structures (Fig. 2**A**). Once the CD spectra of the time-dependent $A\beta_{1-42}$ conformational transition were characterized, we proceeded to analyze the effect of the co-incubation of different molar excesses of ISOAC1 on the variations of the $A\beta_{1-42}$ secondary structure over time. As shown in Fig. 2**B-D** and in Fig. S2, the CD spectra of $A\beta_{1-42}$ in the presence of ISOAC1 at 1:1.25, 1:2.5, and 1:5 Aβ:ISOAC1 molar ratios did not display the characteristic β-sheet pattern after 96 h of incubation (Fig. 2**D** and Fig. S2), suggesting that ISOAC1 can reduce the tendency of $A\beta_{1-42}$ to aggregate and form β-sheet structures. Interestingly, the recorded CD spectra of $A\beta_{1-42}$ with a 5-fold molar excess of ISOAC1 exhibited the strongest negative ellipticity among all the tested ratios (Fig. 2**D** and Fig. S2C).

To obtain quantitative information about the ability of ISOAC1 to affect the variations in the content of different $A\beta_{1-42}$ secondary structures, the experimental CD spectra were subjected to deconvolution

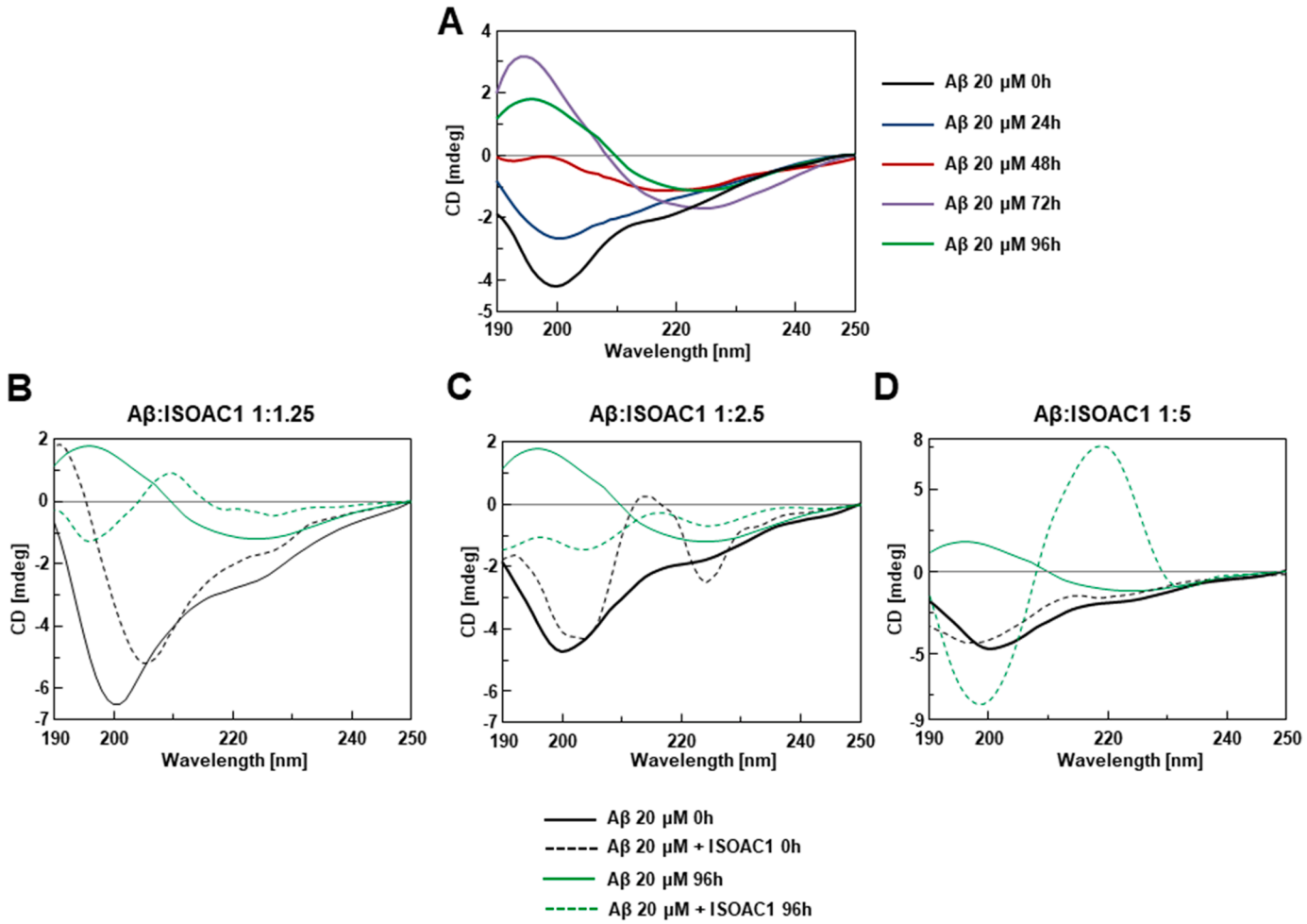

Fig. 2. ISOAC1 inhibits the $A\beta_{1-42}$ conformational transition to β-sheet structures. Time-dependent far-UV CD spectra of the freshly prepared 20 μM-$A\beta_{1-42}$ incubated in 10 mM K^+ buffer (9 mM KCl and 1 mM KH_2PO_4, pH 7.4) at 37 °C analyzed after 0, 24, 48, 72, and 96 h (**A**). Far-UV CD spectra of freshly prepared 20 μM-$A\beta_{1-42}$ incubated in the absence (solid lines) and in the presence (dashed lines) of ISOAC1 at the indicated molar ratios analyzed after 0 and 96 h (**B-D**).

analyses using the Bestsel algorithm [74]. The values of the determined β-sheet secondary structures of $A\beta_{1-42}$ after 0 and 96 h of incubation in the presence of ISOAC1 at 1:1.25, 1:2.5, and 1:5 Aβ:ISOAC1 molar ratios are represented in Table 1. In general, we found a decrease in the β-sheet content already at 0 h for all the three tested ratios. However, a major effect in the β-sheet content reduction was observed after 96 h for 1:2.5 and 1:5 ratios but not for 1:1.25. Remarkably, the decrease in the β-sheet content, which is typically associated to the $A\beta_{1-42}$ aggregation inhibition [60,61,73],[75], was accompanied by an increase in the turn content, which instead reportedly decreases during the Aβ aggregation [76]. These results showed that ISOAC1 at 1:2.5 and 1:5 Aβ:ISOAC1 molar ratios was able to inhibit the conformational transition of $A\beta_{1-42}$ into β-sheet structures and further demonstrated the inhibitory activity of ISOAC1 on the $A\beta_{1-42}$ aggregation, although the concentration-dependence of the anti-aggregating effect emerged in the ThT experiments was only partially confirmed.

Table 1
Variation in $A\beta_{42}$ structure content determined by ISOAC1 as calculated by Bestsel algorithm.

Aβ:ISOAC1 ratio	1:1.25		1:2.5		1:5	
Time/h	0	96	0	96	0	96
Δ_{beta} content	−4.2 ±0.4	+5.0 ±0.1	−3.3 ±0.2	−8.2 ±0.1	−4.1 ±0.1	−7.7 ±0.4
Δ_{turn} content	+4.1 ±0.4	−2.2 ±0.1	+1.1 ±0.2	+3.4 ±0.1	−0.4 ±0.1	+4.0 ±0.4

3.3. *The β-diketone-3-substituted isoindolinone ISOAC1 binds to both monomeric and protofibrillar $A\beta_{1-42}$ structures establishing a hydrophobic interaction with PHE19 residue of $A\beta_{1-42}$*

To understand whether and how the structure of ISOAC1 (Fig. 3**A**) might underlie its anti-amyloidogenic activity, we performed molecular docking studies with the 1-Click (Mcule) software. The binding interactions were studied using ISOAC1 as ligand and the monomeric $A\beta_{1-42}$ structure as target. The chosen monomeric structure, PDB ID: 1IYT, which is routinely used to study the interaction of the $A\beta_{1-42}$ monomer with candidate inhibitors [44, 77–79], consists of two α-helix regions (involving residues 8–25 and 28–38) and a turn region (formed by residues 26–27). Interestingly, we found that the binding energy of the complex between ISOAC1 and the $A\beta_{1-42}$ monomer was −4.7 kcal/mol, hence suggesting the ability of ISOAC1 to bind to $A\beta_{1-42}$. The complex was characterized by a H-bonding between one of the two ketone oxygens of ISOAC1 and the GLN15 guanidinium hydrogen of $A\beta_{1-42}$ (Fig. 3**B-D**). Very interestingly, a hydrophobic interaction between ISOAC1 and the PHE19 of $A\beta_{1-42}$ was also found (Fig. 3**B-D**). In particular, the indole moiety of ISOAC1 and the PHE19 aromatic ring were found to be coplanar (Fig. 3**B-D**), hence suggesting a stacking effect between these moieties, which was further confirmed by the pose analysis performed with the ProteinPlus software (Fig. 3**D**). This molecular interaction likely resulted in changes in Aβ aggregation and

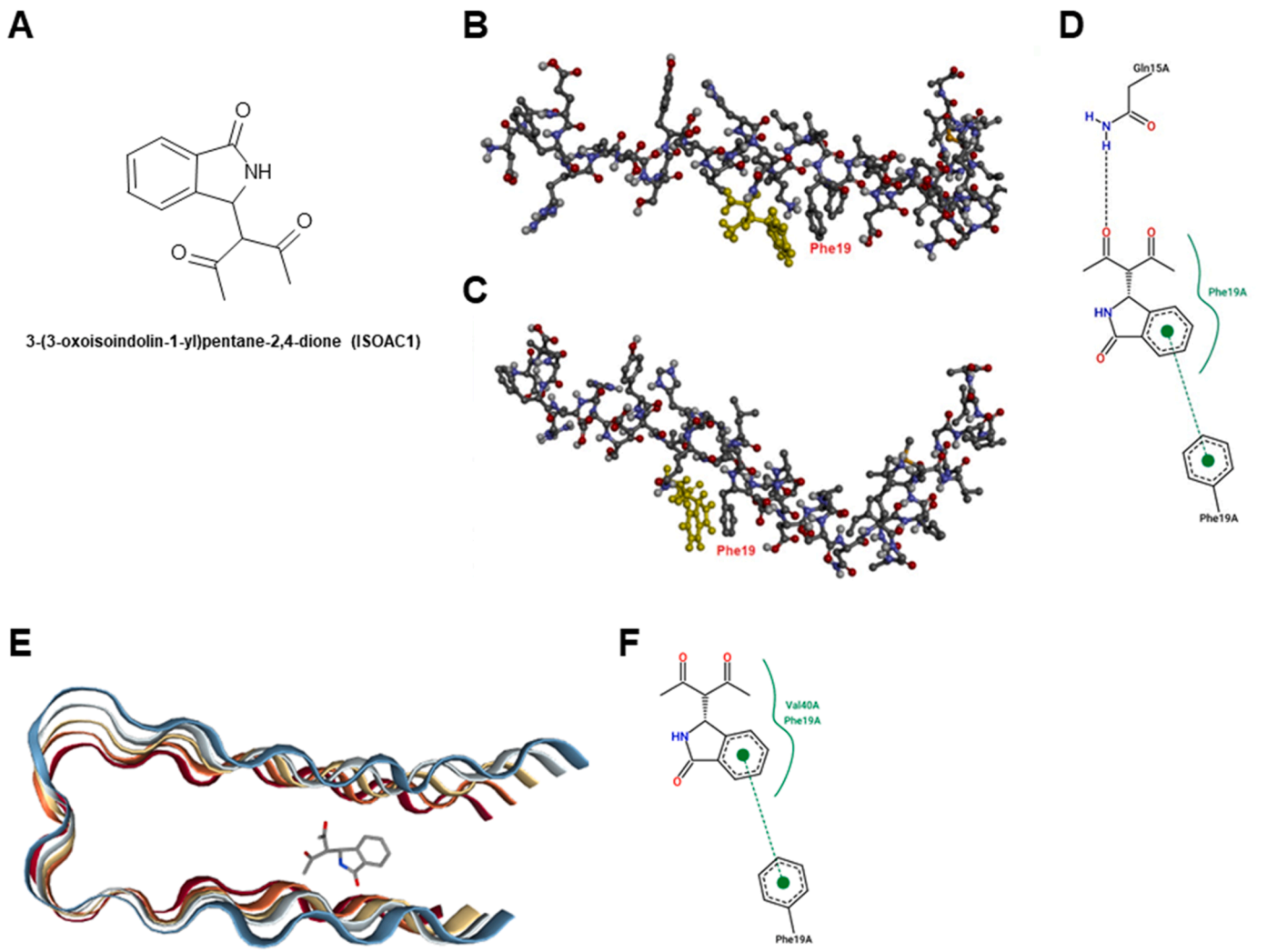

Fig. 3. ISOAC1 is able to bind to both monomeric and protofibrillar Aβ_{1-42} structures. Pose views of the complex formed between ISOAC1 and Aβ_{1-42} monomer (PDB ID: 1IYT) as predicted by docking with 1-Click (Mcule) software (**A,B**). 2D peptide-ligand interaction diagram obtained by ProteinPlus with the docked structure of the complex formed by ISOAC1 and Aβ_{1-42} monomer (**C**). Pose view of the complex formed between ISOAC1 and Aβ_{1-42} protofibril (PDB ID:2BEG, represented as cartoon) as predicted by docking with 1-Click (Mcule) software (**D**). Details of the hydrophobic and aromatic binding between ISOAC1 and Aβ_{1-42} protofibril in the 2D peptide-ligand interaction diagram obtained by ProteinPlus (**E**).

alteration in the secondary structure of Aβ.

To further investigate the ability of ISOAC1 to interact with prefibrillar structures of Aβ_{1-42}, we performed a docking experiment between ISOAC1 and a pentameric, protofibrillar Aβ_{1-42}structure, PDB ID:2BEG, which has been largely used to study the dynamics of Aβ aggregation and the anti-aggregating ability of candidate compounds [80–84]. The binding energy of the complex between ISOAC1 and the Aβ_{1-42} pentamer was −5.3 kcal/mol. Unlike for the ISOAC1-monomer complex, no H-bonding was found between ISOAC1 and the pentameric Aβ_{1-42} structure. However, a partial coplanarity between the isoindolinone ring and the phenyl moiety of the PHE19 residue was noticed (Fig. 3**E**), hence suggesting the presence of stacking interactions between ISOAC1 and the PHE19 residue. The pose analysis by ProteinPlus software confirmed this hypothesis and revealed that ISOAC1 was involved in two hydrophobic interactions with the VAL40 and PHE19 residues and in an aromatic interaction with the PHE19 residue (Fig. 3**F**).

Of note, the presence of PHE19 is a striking feature of the hydrophobic core ^{16}KLVFFA^{21} of both Aβ_{1-40} and the Aβ_{1-42}, which has been clearly demonstrated to play a key role in the formation of toxic oligomers by functioning as a self-recognition element [85–87]. Indeed, several studies reported that the PHE19 substitution with either natural or non-natural amino acids led to significant alterations in the Aβ fibrillation kinetics or to drastic changes in its secondary structure [88, 89]. In some cases, the PHE19 substitution completely abolished the Aβ_{1-40} cellular toxicity without inhibiting fibrillation, by perturbing the early folding contact between PHE19 and LEU34 and likely steering the aggregation process through different, less-toxic oligomers [89–91]. Coherently, many small molecules displaying anti-aggregating activity *in vitro* stabilize the Aβ native helical conformation and inhibit the formation of aggregation-prone β-sheet conformation by interacting with the KLVFF motif [78,92]. Moreover, considered that the aromatic residues of the fibril core region are critical for fibril stability [84], compounds interacting with these residues can interrupt hydrophobic interactions and destabilize fibril structure [93].

Based on these considerations, we hypothesized that the ISOAC1 binding mode prevented the formation of crucial intra- and interpeptide π–π stacking interactions ultimately impeding aggregation. In addition, our results suggest that the ISOAC1 interaction with the PHE19 residue of Aβ fibrils can disrupt key interchain stacking interactions, hence preventing fibrils from being elongated.

3.4. The β-diketone-3-substituted isoindolinone ISOAC1 inhibits the detrimental increase of $[Ca^{2+}]_i$ induced by $A\beta_{1-42}$ in primary cortical neurons

It is widely known that the pathogenicity of the Aβ peptide is largely determined by its ability to interfere with multiple mechanisms controlling the ionic homeostasis of brain cells [94]. In this context, the disruption of the Ca^{2+} handling machinery has received the greatest attention and is still the object of intense investigation, since it has been linked to cognitive decline and memory loss [95]. Many studies have focused on the correlation between Ca^{2+} dyshomeostasis and the Aβ aggregation states and, although conflicting results have emerged, solid demonstrations have been provided that Aβ fibrils are not able to disturb neuronal Ca^{2+} signaling [96]. By contrast, low-n Aβ oligomers like dimers and trimers were shown to be the most effective species in eliciting acute cytosolic Ca^{2+} increases through multiple mechanisms, including the formation of cation-permeable membrane pores, and the activation of both cell surface receptors such as the NMDA receptors and endoplasmic reticulum Ca^{2+} release [97–99]. Importantly, these early aberrant Ca^{2+} responses translate into a cascade of events including the prolonged failure of the Ca^{2+} homeostatic machinery, mitochondrial dysfunction, increased ROS production, and apoptotic cell death, among others [100,101].

In the light of these considerations, we examined whether ISOAC1 was able to protect neurons against the $A\beta_{1-42}$ injury firstly by evaluating its ability to interfere with the increase of $[Ca^{2+}]_i$ induced by low-n $A\beta_{1-42}$ oligomers. To this aim, we applied to Fura-2-loaded cortical neurons an unaged $A\beta_{1-42}$ preparation (5 μM), enriched in both monomers and low-n oligomers (Fig. 1**B**), in the presence and in the absence of 25 μM ISOAC1, and assessed the alteration of the intracellular Ca^{2+} levels by monitoring the change in $[Ca^{2+}]_i$. Importantly, we found that the presence of ISOAC1 significantly reduced the $[Ca^{2+}]_i$ increase induced by $A\beta_{1-42}$ oligomers (Fig. 4 **A,B**). This result can be ascribable to the rapid capability of ISOAC1 to inhibit the formation of LMW $A\beta_{1-42}$ species with a β-sheet secondary structure, a conformational property reportedly decisive not only for the Aβ aggregation process but also for the assembly of Aβ channel-pores on the plasma membrane [102,103]. Of note, this hypothesis is in line with the observation that ISOAC1 was able to reduce the β-sheet content already at 0 h of incubation, namely at the beginning of the aggregation process (Table 1 and Fig. 2 B). Nevertheless, it is worth mentioning that the PHE19 residue was demonstrated to be critical for the formation of Ca^{2+}-permeable Aβ channel-pores, as its substitution with proline resulted in decreased Aβ pore conductivity and cellular toxicity [104,105]. In view of this, it can be hypothesized that the hydrophobic interaction of ISOAC1 with the PHE19 residue might serve to interfere with multiple mechanisms ultimately attenuating the $A\beta_{1-42}$-mediated Ca^{2+}signaling.

3.5. The β-diketone-3-substituted isoindolinone ISOAC1 prevents the $A\beta_{1-42}$-induced mitochondrial dysfunction in primary cortical neurons

Based on the results described above, we tested ISOAC1 for its neuroprotective effect in rat primary cortical neurons after 24 h of exposure to unaged $A\beta_{1-42}$ preparations. In order to exclude any cellular toxicity of our compound, we first exposed primary cortical neurons to increasing concentrations of ISOAC1 (5, 25, 50, and 100 μM) and assessed the mitochondrial dehydrogenase activity reduction after 24 h as index of a cytotoxic response. Importantly, no significant cytotoxicity was observed for ISOAC1 at any of the tested concentrations (Fig. 5**A**). Then, we evaluated whether the co-treatment with ISOAC1 could be protective against the $A\beta_{1-42}$ toxicity in primary cortical neurons. Considered that a ISOAC1 molar concentration 5-fold higher than that of $A\beta_{1-42}$ had demonstrated the greatest efficacy in preventing the $A\beta_{1-42}$ aggregation, we exposed neurons to 25 μM ISOAC1 30 min prior to add 5 μM $A\beta_{1-42}$ to the culture medium. The reduction of the mitochondrial dehydrogenase activity was evaluated through the MTT assay at the end of 24 h of treatment, to allow $A\beta_{1-42}$ to aggregate and be internalized by the neurons. Interestingly, the treatment with $A\beta_{1-42}$ alone induced a significant reduction in the mitochondrial dehydrogenase activity, an effect that was significantly attenuated by the co-treatment with ISOAC1 (Fig. 5**B**).

To evaluate the neuroprotective effect of ISOAC1 against the $A\beta_{1-42}$ toxicity, we also assessed the intracellular ROS levels after 24 h of $A\beta_{1-42}$ treatment. Indeed, along with mitochondrial failure, the increase of ROS

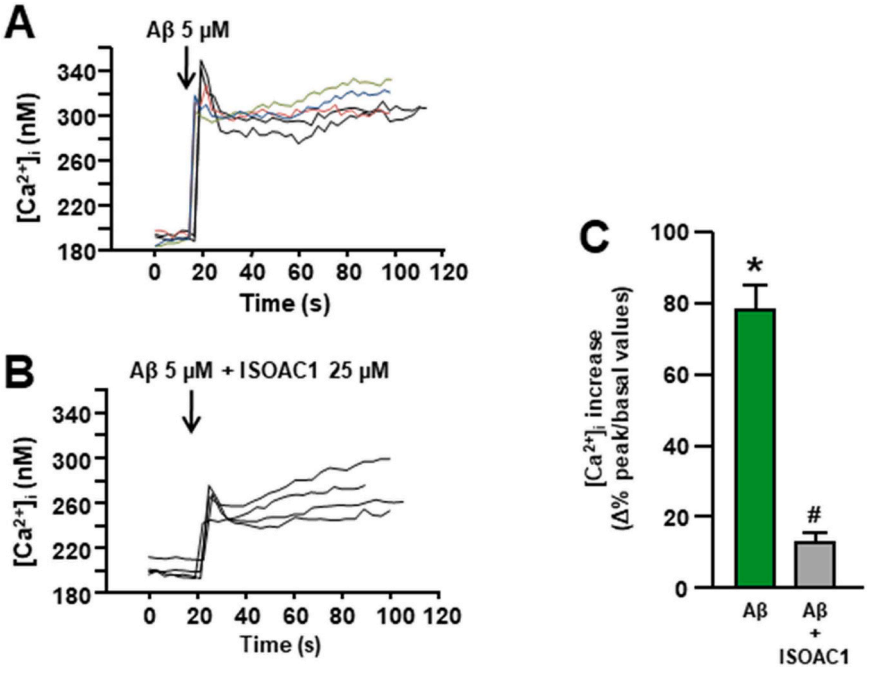

Fig. 4. ISOAC1 prevents the acute $[Ca^{2+}]_i$ increase induced by $A\beta_{1-42}$ in primary cortical neurons loaded with Fura-2. Representative superimposed traces of $[Ca^{2+}]_i$ increase triggered by $A\beta_{1-42}$ (5 μM) under control conditions (**A**) or in presence of ISOAC1 (25 μM) (**B**). Quantification of A and B (**C**). Data are expressed as mean ± S.E.M. of 3 independent experimental sessions ($n = 45$ in A; $n = 48$ in B). * $p < 0.05$ *vs* Control (basal values); # $p < 0.05$ *vs* $A\beta_{1-42}$ alone.

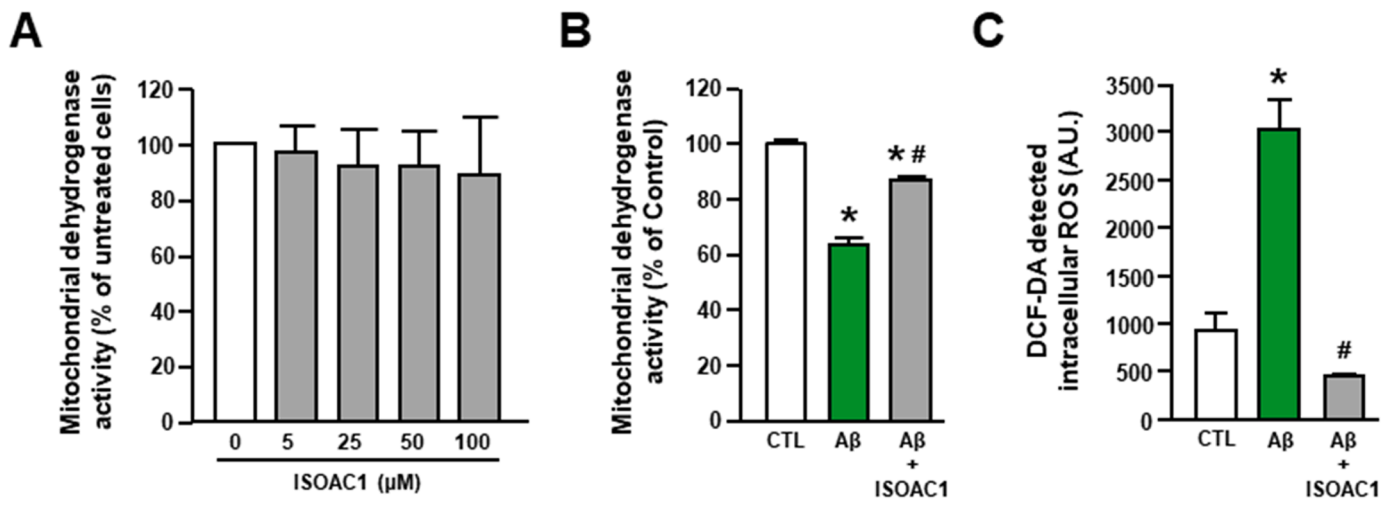

Fig. 5. ISOAC1 protects primary cortical neurons against the $A\beta_{1-42}$-induced reduction of mitochondrial dehydrogenase activity and increase of ROS production. Evaluation of cytotoxicity as mitochondrial dehydrogenase activity reduction in primary cortical neurons after 24 h of exposure to ISOAC1 at different concentrations (5, 25, 50, and 100 μM). Data are expressed as mean ± S.E.M. of 3 independent experimental sessions. (**A**). Evaluation of mitochondrial dehydrogenase activity in primary cortical neurons exposed for 24 h to 5 μM $A\beta_{1-42}$ in the absence and in the presence of 25 μM ISOAC1 (30 min pre-treatment). Data are expressed as mean ± S.E.M. of 3 independent experimental sessions * $p < 0.05$ *vs* Control; # $p < 0.05$ *vs* $A\beta_{1-42}$ alone (B). Quantification of intracellular ROS production by measuring DCFH-DA fluorescence intensity in primary cortical neurons exposed for 24 h to 5 μM $A\beta_{1-42}$ alone or after a 30 min pre-treatment with 25 μM ISOAC1. Data are expressed as mean ± S.E.M. of 3 independent experimental sessions * $p < 0.05$ *vs* Control; # $p < 0.05$ *vs* $A\beta_{1-42}$ alone (C).

production and subsequent oxidative stress are critical downstream events of the Aβ aggregation and accumulation at the cellular level, and are widely believed to play a crucial role in the AD pathogenesis [106, 107]. In particular, we assessed ROS levels in primary cortical neurons by using the ROS-sensitive fluorescent probe DCFH-DA after 24 h of exposure to 5 μM $A\beta_{1-42}$ in the presence and in the absence of 25 μM ISOAC1. As expected, we observed a significant increase of ROS levels in neurons treated with $A\beta_{1-42}$ alone. Of note, the co-treatment with ISOAC1 completely inhibited the increase of ROS production induced by $A\beta_{1-42}$ (Fig. 5**C**).

3.6. The β-diketone-3-substituted isoindolinone ISOAC1 reduced the $A\beta_{1-42}$ accumulation in primary cortical neurons

Previous studies have clearly demonstrated that the β-sheet conformation is a pre-requisite for the $A\beta_{1-42}$ cellular uptake. It was shown that β-sheet-rich aggregates, rather than $A\beta_{1-42}$ monomers, are efficiently taken up by cells through vesicle endocytosis. More importantly, the formation and subsequent uptake of β-sheet-rich aggregates directly correlate with the cell metabolic inhibition [108]. In the light of this evidence, we also investigated whether ISOAC1 was able to reduce $A\beta_{1-42}$ intraneuronal accumulation, a mechanism that could contribute to its neuroprotective effect. To this aim, after exposing the neurons to $A\beta_{1-42}$ for 24 h we performed immunofluorescence experiments with the anti-$A\beta_{1-42}$ (D54D2) primary antibody. We used 24 h of incubation since it was reported that the amount of internalized Aβ is time-dependent and the highest intracellular Aβ signal has been found after 24 h [108]. As expected, the neurons treated with $A\beta_{1-42}$ alone displayed an intense $A\beta_{1-42}$ immunosignal both at the perikaryon and neurite level, observable intracellularly and in association with the neuronal plasma membrane (Fig. 6**A**). Interestingly, quantitative analyses indicated that the $A\beta_{1-42}$ immunofluorescence was significantly lower in the neurons pre-treated with ISOAC1 in comparison with the neurons treated with $A\beta_{1-42}$ alone, hence suggesting that ISOAC1 was able to reduce $A\beta_{1-42}$ accumulation (Fig. 6**B**).

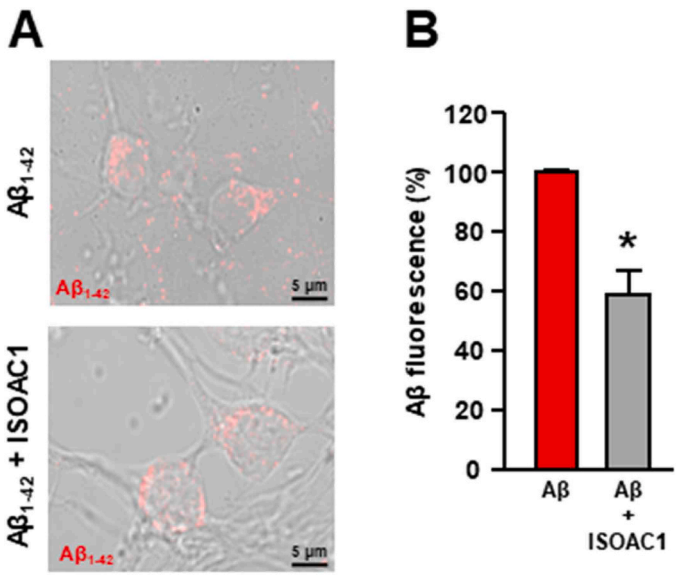

Fig. 6. ISOAC1 reduces $A\beta_{1-42}$ accumulation in primary cortical neurons. Representative confocal images showing $A\beta_{1-42}$ immunostaining in primary cortical neurons exposed for 24 h to 5 μM $A\beta_{1-42}$ in the absence and in the presence of 25 μM ISOAC1 (30 min pre-treatment) (**A**), and quantification of $A\beta_{1-42}$ immunofluorescence. Data are expressed as mean ± S.E.M. of 3 independent experimental sessions * $p < 0.05$ *vs* $A\beta_{1-42}$ alone ($n = 30$ neurons for each group of three experimental sessions) (**B**).

4. Conclusions

In the present study, we performed *in silico* and *in vitro* analyses to investigate the selected compound, ISOAC1, for its putative ability to inhibit the $A\beta_{1-42}$ aggregation and subsequent neuronal toxicity. Importantly, we found that ISOAC1 was able to inhibit the aggregation of $A\beta_{1-42}$ by blocking the conversion from its native conformation to a β-sheet secondary structure, which is a key aspect of the aggregation process [109]. In line with several studies showing that the β-sheet-rich oligomers are the most toxic Aβ species [110,111], we found that the $A\beta_{1-42}$ samples aggregated in the presence of ISOAC1 were less toxic than those incubated alone, consistently with a lower content of β-sheet-rich structures. Moreover, we have also reported that ISOAC1

was able to protect primary cortical neurons from the $A\beta_{1-42}$ injury, by counteracting the early steps of $A\beta_{1-42}$ toxicity, such as intracellular Ca^{2+} level elevations, mitochondrial activity reduction, and increase of ROS production, as well as by reducing $A\beta_{1-42}$ accumulation.

Intriguingly, our *in silico* studies revealed a hydrophobic interaction between ISOAC1 and the PHE19 residue of the $A\beta_{1-42}$ monomer. In addition, we also found that ISOAC1 was able to form hydrophobic and aromatic interactions with a pentameric, protofibrillar form of $A\beta_{1-42}$, hence suggesting its ability to destabilize fibrillar structures and prevent their further elongation. Therefore, it is possible to hypothesize that the ISOAC1 interaction with the $A\beta_{1-42}$ structure, especially with the PHE19 residue, might underlie its anti-amyloidogenic activity by interfering with multiple steps of the cell-mediated amyloidogenesis. Since previous analyses showed that ISOAC1 is characterized by drug-likeness and no toxicity, we believed that it could serve as an effective and promising candidate for the development of $A\beta_{1-42}$-targeting strategies in the AD treatment.

Funding

This study was supported by the following grants: Programma di Finanziamento LInea-1 54_2020_FRA to AP; Programma di Finanziamento Linea-1 54_2020_FRA to AS. University of Salerno and MUR for financial support (FARB) to AM.

CRediT authorship contribution statement

Ilaria Piccialli: Conceptualization, Methodology, Investigation, Formal analysis, Writing – original draft, Writing – review & editing. **Francesca Greco, Maria Josè Sisalli, Valentina Tedeschi, Antonia Di Mola**: Investigation. **Giovanni Roviello, Nicola Borbone, Giorgia Oliviero**: Methodology, Investigation, Formal analysis, Writing – original draft. **Vincenzo De Feo**: Writing – review & editing. **Agnese Secondo**: Investigation, Formal analysis, Writing – review & editing. **Antonio Massa, Anna Pannaccione**: Formal analysis, Writing – review & editing, Supervision. All authors have read and agreed to the published version of the manuscript.

Declaration of Competing Interest

The authors declare that there are no conflicts of interests.

Data Availability

Data will be made available on request.

Acknowledgment

The authors thank all of the participants for their interest in this study and express their gratitude to Gergely Prikler and Gergely Takács (https://mcule.com, Mcule team, Hungary) for their kind support with the 1-Click Mcule online platform.

Appendix A. Supporting information

Supplementary data associated with this article can be found in the online version at doi:10.1016/j.biopha.2023.115745.

References

[1] H.W. Querfurth, F.M. LaFerla, Alzheimer's disease, N. Engl. J. Med 362 (2010) 329–344, https://doi.org/10.1056/NEJMra0909142.
[2] D.J. Selkoe, Alzheimer's disease: genes, proteins, and therapy, Physiol. Rev. 81 (2001) 741–766, https://doi.org/10.1152/physrev.2001.81.2.741.
[3] J.C. Morris, M. Storandt, D.W. McKeel Jr, E.H. Rubin, J.L. Price, E.A. Grant, L. Berg, Cerebral amyloid deposition and diffuse plaques in "normal" aging: evidence for presymptomatic and very mild Alzheimer's disease, Neurology 46 (1996) 707–719, https://doi.org/10.1212/wnl.46.3.707.
[4] G.B. Irvine, O.M. El-Agnaf, G.M. Shankar, D.M. Walsh, Protein aggregation in the brain: the molecular basis for Alzheimer's and Parkinson's diseases, Mol. Med. 14 (2008) 451–464, https://doi.org/10.2119/2007-00100.Irvine.
[5] A. Lorenzo, B.A. Yankner, Beta-amyloid neurotoxicity requires fibril formation and is inhibited by congo red, Proc. Natl. Acad. Sci. U. S. A. 91 (1994) 12243–12247, https://doi.org/10.1073/pnas.91.25.12243.
[6] K. Ueda, S. Shinohara, T. Yagami, K. Asakura, K. Kawasaki, Amyloid beta protein potentiates Ca2+ influx through L-type voltage-sensitive Ca2+ channels: a possible involvement of free radicals, J. Neurochem. 68 (1997) 265–271, https://doi.org/10.1046/j.1471-4159.1997.68010265.x.
[7] M. Shoji, T.E. Golde, J. Ghiso, T.T. Cheung, S. Estus, L.M. Shaffer, X.D. Cai, D. M. McKay, R. Tintner, B. Frangione, et al., Production of the Alzheimer amyloid beta protein by normal proteolytic processing, Science 258 (1992) 126–129, https://doi.org/10.1126/science.1439760.
[8] C. Priller, T. Bauer, G. Mitteregger, B. Krebs, H.A. Kretzschmar, J. Herms, Synapse formation and function is modulated by the amyloid precursor protein, J. Neurosci. 26 (2006) 7212–7221, https://doi.org/10.1523/JNEUROSCI.1450-06.2006.
[9] R. Pellarin, A. Caflisch, Interpreting the aggregation kinetics of amyloid peptides, J. Mol. Biol. 360 (2006) 882–892, https://doi.org/10.1016/j.jmb.2006.05.033.
[10] M.P. Lambert, K.L. Viola, B.A. Chromy, L. Chang, T.E. Morgan, J. Yu, D.L. Venton, G.A. Krafft, C.E. Finch, W.L. Klein, Vaccination with soluble Abeta oligomers generates toxicity-neutralizing antibodies, J. Neurochem. 79 (2001) 595–605, https://doi.org/10.1046/j.1471-4159.2001.00592.x.
[11] D.J. Selkoe, Soluble oligomers of the amyloid beta-protein impair synaptic plasticity and behavior, Behav. Brain Res. 192 (2008) 106–113, https://doi.org/10.1016/j.bbr.2008.02.016.
[12] K. Broersen, F. Rousseau, J. Schymkowitz, The culprit behind amyloid beta peptide related neurotoxicity in Alzheimer's disease: oligomer size or conformation? Alzheimers Res. Ther. 2 (2010) 12, https://doi.org/10.1186/alzrt36.
[13] D.J. Selkoe, Translating cell biology into therapeutic advances in Alzheimer's disease, Nature 399 (1999) A23–A31, https://doi.org/10.1038/399a023.
[14] A. Miranda, E. Montiel, H. Ulrich, C. Paz, Selective secretase targeting for Alzheimer's disease therapy, J. Alzheimers Dis. 81 (2021) 1–17, https://doi.org/10.3233/JAD-201027.
[15] S.H. Barage, K.D. Sonawane, Amyloid cascade hypothesis: pathogenesis and therapeutic strategies in Alzheimer's disease, Neuropeptides 52 (2015) 1–18, https://doi.org/10.1016/j.npep.2015.06.008.
[16] A. Gea-González, S. Hernández-García, P. Henarejos-Escudero, P. Martínez-Rodríguez, F. García-Carmona, F. Gandía-Herrero, Polyphenols from traditional Chinese medicine and Mediterranean diet are effective against Aβ toxicity *in vitro* and *in vivo* in *Caenorhabditis elegans*, Food Funct. 13 (2022) 1206–1217, https://doi.org/10.1039/d1fo02147h.
[17] D.A. Loeffler, Antibody-mediated clearance of brain amyloid-β: mechanisms of action, effects of natural and monoclonal anti-Aβ antibodies, and downstream effects, J. Alzheimers Dis. Rep. 7 (2023) 873–899, https://doi.org/10.3233/ADR-230025.
[18] A. Francioso, P. Punzi, A. Boffi, C. Lori, S. Martire, C. Giordano, M. D'Erme, L. Mosca, β-sheet interfering molecules acting against β-amyloid aggregation and fibrillogenesis, Bioorg. Med. Chem. 23 (2015) 1671–1683, https://doi.org/10.1016/j.bmc.2015.02.041.
[19] S. Chimon, M.A. Shaibat, C.R. Jones, D.C. Calero, B. Aizezi, Y. Ishii, Evidence of fibril-like β-sheet structures in a neurotoxic amyloid intermediate of Alzheimer's β-amyloid, Nat. Struct. Mol. Biol. 15 (2007) 1157–1164, https://doi.org/10.1038/nsmb1345.
[20] Stroud J.C., Liu C., Teng P.K., Eisenberg D. Toxic fibrillar oligomers of amyloid-β have cross-β structure. Proc. Natl. Acad. Sci. U. S. A. 109 (2012) 7717–7722. doi: 10.1073/pnas.1203193109.
[21] C. Hilbich, B. Kisters-Woike, J. Reed, C.L. Masters, K. Beyreuther, Substitutions of hydrophobic amino acids reduce the amyloidogenicity of Alzheimer's disease beta A4 peptides, J. Mol. Biol. 228 (1992) 460–473, https://doi.org/10.1016/0022-2836(92)90835-8.
[22] G.M.L. Consoli, R. Tosto, A. Baglieri, S. Petralia, T. Campagna, G. Di Natale, S. Zimbone, M.L. Giuffrida, G. Pappalardo, Novel peptide-calix[4]arene conjugate inhibits Aβ aggregation and rescues neurons from Aβ's oligomers cytotoxicity *In Vitro*, ACS Chem. Neurosci. 12 (2021) 1449–1462, https://doi.org/10.1021/acschemneuro.1c00117.
[23] N. Innocent, N. Evans, C. Hille, S. Wonnacott, Oligomerisation differentially affects the acute and chronic actions of amyloid-beta in vitro, Neuropharmacology 59 (2010) 343–352, https://doi.org/10.1016/j.neuropharm.2010.04.003.
[24] J. Liu, W. Wang, Q. Zhang, S. Zhang, Z. Yuan, Study on the efficiency and interaction mechanism of a decapeptide inhibitor of β-amyloid aggregation, Biomacromolecules 15 (2014) 931–939, https://doi.org/10.1021/bm401795e.
[25] I. Piccialli, V. Tedeschi, L. Caputo, S. D'Errico, R. Ciccone, V. De Feo, A. Secondo, A. Pannaccione, Exploring the therapeutic potential of phytochemicals in alzheimer's disease: focus on polyphenols and monoterpenes, Front. Pharmacol. 13 (2022), 876614, https://doi.org/10.3389/fphar.2022.876614.
[26] L. Di Matteo, O. Christodoulakis, R. Filosa, P. De Caprariis, A. Di Mola, E. Vasca, A. Massa, New chelating agents for Cu(II), Fe(III), Al(III), and Zn(II) based on β-diketonate-3-substituted phthalide (isobenzofuranone) and isoindolinone, J. Coord. Chem. (2014), https://doi.org/10.1080/00958972.2014.939075.

[27] V. More, A. Di Mola, M. Perillo, P. De Caprariis, R. Filosa, A. Peduto, A. Massa, The aldol addition of readily enolizable 1,3-dicarbonyl compounds to 2-cyanobenzaldehyde in the synthesis of 3-substituted isoindolinones, Synthesis 18 (2011) 3027.
[28] M.S. Mousavi, A. Di Mola, A. Massa, Multifaceted behavior of 2-cyanobenzaldehyde and 2-acylbenzonitriles in the synthesis of isoindolinones, phthalides and related heterocycles, Eur. J. Org. Chem. 26 (2023), e202300289, https://doi.org/10.1002/ejoc.202300289.
[29] A. Więckowska, K. Więckowski, M. Bajda, B. Brus, K. Sałat, P. Czerwińska, S. Gobec, B. Filipek, B. Malawska, Synthesis of new N-benzylpiperidine derivatives as cholinesterase inhibitors with β-amyloid anti-aggregation properties and beneficial effects on memory in vivo, Bioorg. Med. Chem. 23 (2015) 2445–2457, https://doi.org/10.1016/j.bmc.2015.03.051.
[30] R.T. Kareem, F. Abedinifar, E.A. Mahmood, A.G. Ebadi, F. Rajabi, E. Vessally, The recent development of donepezil structure-based hybrids as potential multifunctional anti-Alzheimer's agents: highlights from 2010 to 2020, RSC Adv. 11 (2021) 30781–30797, https://doi.org/10.1039/d1ra03718h.
[31] N. Guzior, A. Wieckowska, D. Panek, B. Malawska, Recent development of multifunctional agents as potential drug candidates for the treatment of Alzheimer's disease, Curr. Med. Chem. 22 (2015) 373–404, https://doi.org/10.2174/0929867321666141106122628.
[32] R. Ciccone, C. Franco, I. Piccialli, F. Boscia, A. Casamassa, V. de Rosa, P. Cepparulo, M. Cataldi, L. Annunziato, A. Pannaccione, Amyloid β-induced upregulation of nav1.6 underlies neuronal hyperactivity in Tg2576 Alzheimer's disease mouse model, Sci. Rep. 9 (2019) 13592, https://doi.org/10.1038/s41598-019-50018-1.
[33] R. Ciccone, I. Piccialli, P. Grieco, F. Merlino, L. Annunziato, A. Pannaccione, Synthesis and pharmacological evaluation of a novel peptide based on *Anemonia sulcata* BDS-I toxin as a new K_V3.4 inhibitor exerting a neuroprotective effect against amyloid-β peptide, Front. Chem. 7 (2019) 479, https://doi.org/10.3389/fchem.2019.00479.
[34] W.B. Stine Jr, K.N. Dahlgren, G.A. Krafft, M.J. LaDu, In vitro characterization of conditions for amyloid-beta peptide oligomerization and fibrillogenesis, J. Biol. Chem. 278 (2003) 11612–11622, https://doi.org/10.1074/jbc.M210207200.
[35] K. Broersen, W. Jonckheere, J. Rozenski, A. Vandersteen, K. Pauwels, A. Pastore, F. Rousseau, J. Schymkowitz, A standardized and biocompatible preparation of aggregate-free amyloid beta peptide for biophysical and biological studies of Alzheimer's disease, Protein Eng. Des. Sel. 24 (2011) 743–750, https://doi.org/10.1093/protein/gzr020.
[36] C. Xue, T.Y. Lin, D. Chang, Z. Guo, Thioflavin T as an amyloid dye: fibril quantification, optimal concentration and effect on aggregation, R. Soc. Open Sci. 4 (2017) J160696, https://doi.org/10.1098/rsos.160696.
[37] D. Jiang, I. Rauda, S. Han, S. Chen, F. Zhou, Aggregation pathways of the amyloid β(1-42) peptide depend on its colloidal stability and ordered β-sheet stacking, Langmuir 28 (2012) 12711–12721, https://doi.org/10.1021/la3021436.
[38] H.M. Berman, T. Battistuz, T.N. Bhat, W.F. Bluhm, P.E. Bourne, K. Burkhardt, Z. Feng, G.L. Gilliland, L. Iype, S. Jain, P. Fagan, J. Marvin, D. Padilla, V. Ravichandran, B. Schneider, N. Thanki, H. Weissig, J.D. Westbrook, C. Zardecki, The protein data bank, Acta Crystallogr. D. Biol. Crystallogr. 58 (2002) 899–907, https://doi.org/10.1107/s0907444902003451.
[39] R. Kiss, M. Sandor, F.A. Szalai, http://Mcule.com: a public web service for drug discovery, J. Chemin.-. 4 (2012) P17, https://doi.org/10.1186/1758-2946-4-S1-P17.
[40] V. Potemkin, A. Potemkin, M. Grishina, Internet resources for drug discovery and design, Curr. Top. Med. Chem. 18 (2018) 1955–1975, https://doi.org/10.2174/1568026619666181129142127.
[41] M.A. Fik-Jaskółka, A.F. Mkrtchyan, A.S. Saghyan, R. Palumbo, A. Belter, L. A. Hayriyan, H. Simonyan, V. Roviello, G.N.Spectroscopic Roviello, and SEM evidences for G4-DNA binding by a synthetic alkyne-containing amino acid with anticancer activity, Spectrochim. Acta A: Mol. Biomol. Spectrosc. 229 (2020), 117884, https://doi.org/10.1016/j.saa.2019.117884.
[42] M.A. Fik-Jaskółka, A.F. Mkrtchyan, A.S. Saghyan, R. Palumbo, A. Belter, L. A. Hayriyan, H. Simonyan, V. Roviello, G.N. Roviello, Biological macromolecule binding and anticancer activity of synthetic alkyne-containing L-phenylalanine derivatives, Amino Acids 52 (2020) 755–769, https://doi.org/10.1007/s00726-020-02849-w.
[43] O. Trott, A.J. Olson, AutoDock Vina: improving the speed and accuracy of docking with a new scoring function, efficient optimization, and multithreading, J. Comput. Chem. 31 (2010) 455–461, https://doi.org/10.1002/jcc.21334.
[44] A. Verma, A. Kumar, M. Debnath, Molecular docking and simulation studies to give insight of surfactin amyloid interaction for destabilizing Alzheimer's Aβ42 protofibrils, Med. Chem. Res. 25 (2016) 1616–1622.
[45] R. Sirabella, A. Secondo, A. Pannaccione, A. Scorziello, V. Valsecchi, A. Adornetto, L. Bilo, G. Di Renzo, L. Annunziato, Anoxia-induced NF-kappaB-dependent upregulation of NCX1 contributes to Ca2+ refilling into endoplasmic reticulum in cortical neurons, Stroke 40 (2009) 922–929, https://doi.org/10.1161/STROKEAHA.108.531962.
[46] M.J. Sisalli, A. Secondo, A. Esposito, V. Valsecchi, C. Savoia, G.F. Di Renzo, L. Annunziato, A. Scorziello, Endoplasmic reticulum refilling and mitochondrial calcium extrusion promoted in neurons by NCX1 and NCX3 in ischemic preconditioning are determinant for neuroprotection, Cell. Death Differ. 21 (2014) 1142–1149, https://doi.org/10.1038/cdd.2014.32.
[47] A. Secondo, T. Petrozziello, V. Tedeschi, F. Boscia, A. Vinciguerra, R. Ciccone, A. Pannaccione, P. Molinaro, G. Pignataro, L. Annunziato, ORAI1/STIM1 interaction intervenes in stroke and in neuroprotection induced by ischemic preconditioning through store-operated calcium entry, Stroke 50 (2019) 1240–1249, https://doi.org/10.1161/STROKEAHA.118.024115.
[48] A. Secondo, R.I. Staiano, A. Scorziello, R. Sirabella, F. Boscia, A. Adornetto, V. Valsecchi, P. Molinaro, L.M. Canzoniero, G. Di Renzo, L. Annunziato, BHK cells transfected with NCX3 are more resistant to hypoxia followed by reoxygenation than those transfected with NCX1 and NCX2: Possible relationship with mitochondrial membrane potential, Cell Calcium 42 (2007) 521–535, https://doi.org/10.1016/j.ceca.2007.01.006.
[49] V. Tedeschi, M.J. Sisalli, T. Petrozziello, L.M.T. Canzoniero, A. Secondo, Lysosomal calcium is modulated by STIM1/TRPML1 interaction which participates to neuronal survival during ischemic preconditioning, FASEB J. 35 (2021), e21277, https://doi.org/10.1096/fj.202001886R.
[50] A. Secondo, T. Petrozziello, V. Tedeschi, F. Boscia, A. Vinciguerra, R. Ciccone, A. Pannaccione, P. Molinaro, G. Pignataro, L. Annunziato, ORAI1/STIM1 interaction intervenes in stroke and in neuroprotection induced by ischemic preconditioning through store-operated calcium entry, Stroke 50 (2019) 1240–1249, https://doi.org/10.1161/STROKEAHA.118.024115.
[51] G. Grynkiewicz, M. Poenie, R.Y. Tsien, A new generation of Ca2+ indicators with greatly improved fluorescence properties, J. Biol. Chem. 260 (1985) 3440–3450.
[52] J. Urbanczyk, O. Chernysh, M. Condrescu, J.P. Reeves, Sodium-calcium exchange does not require allosteric calcium activation at high cytosolic sodium concentrations, J. Physiol. 575 (2006) 693–705, https://doi.org/10.1113/jphysiol.2006.113910.
[53] M.J. Sisalli, S. Della Notte, A. Secondo, C. Ventra, L. Annunziato, A. Scorziello, L-Ornithine L-aspartate restores mitochondrial function and modulates intracellular calcium homeostasis in Parkinson's disease models, Cells 11 (2022) 2909, https://doi.org/10.3390/cells11182909.
[54] R. Di Martino, M.J. Sisalli, R. Sirabella, S. Della Notte, D. Borzacchiello, A. Feliciello, L. Annunziato, A. Scorziello, Ncx3-induced mitochondrial dysfunction in midbrain leads to neuroinflammation in striatum of A53t-α-synuclein transgenic old mice, Int. J. Mol. Sci. 22 (2021) 8177, https://doi.org/10.3390/ijms22158177.
[55] A. Livigni, A. Scorziello, S. Agnese, A. Adornetto, A. Carlucci, C. Garbi, I. Castaldo, L. Annunziato, E.V. Avvedimento, A. Feliciello, Mitochondrial AKAP121 links cAMP and src signaling to oxidative metabolism, Mol. Biol. Cell. 17 (2006) 263–271, https://doi.org/10.1091/mbc.e05-09-0827.
[56] A. Scorziello, C. Savoia, M.J. Sisalli, A. Adornetto, A. Secondo, F. Boscia, A. Esposito, E.V. Polishchuk, R.S. Polishchuk, P. Molinaro, A. Carlucci, L. Lignitto, G. Di Renzo, A. Feliciello, L. Annunziato, NCX3 regulates mitochondrial Ca(2+) handling through the AKAP121-anchored signaling complex and prevents hypoxia-induced neuronal death, J. Cell. Sci. 126 (2013) 5566–5577, https://doi.org/10.1242/jcs.129668.
[57] S.H. Han, J.C. Park, I. Mook-Jung, Amyloid β-interacting partners in Alzheimer's disease: from accomplices to possible therapeutic targets, Prog. Neurobiol. 137 (2016) 17–38, https://doi.org/10.1016/j.pneurobio.2015.12.004.
[58] J.A. Cohlberg, J. Li, V.N. Uversky, A.L. Fink, Heparin and other glycosaminoglycans stimulate the formation of amyloid fibrils from alpha-synuclein in vitro, Biochemistry 41 (2002) 1502–1511, https://doi.org/10.1021/bi011711s.
[59] H. LeVine 3rd, Thioflavine T interaction with synthetic Alzheimer's disease beta-amyloid peptides: detection of amyloid aggregation in solution, Protein Sci. 2 (1993) 404–410, https://doi.org/10.1002/pro.5560020312.
[60] O.N. Antzutkin, J.J. Balbach, R.D. Leapman, N.W. Rizzo, J. Reed, R. Tycko, Multiple quantum solid-state NMR indicates a parallel, not antiparallel, organization of beta-sheets in Alzheimer's beta-amyloid fibrils, Proc. Natl. Acad. Sci. U. S. A. 97 (2000) 13045–13050, https://doi.org/10.1073/pnas.230315097.
[61] A.T. Petkova, G. Buntkowsky, F. Dyda, R.D. Leapman, W.M. Yau, R. Tycko, Solid state NMR reveals a pH-dependent antiparallel beta-sheet registry in fibrils formed by a beta-amyloid peptide, J. Mol. Biol. 335 (2004) 247–260, https://doi.org/10.1016/j.jmb.2003.10.044.
[62] A.R. Ladiwala, J.C. Lin, S.S. Bale, A.M. Marcelino-Cruz, M. Bhattacharya, J. S. Dordick, P.M. Tessier, Resveratrol selectively remodels soluble oligomers and fibrils of amyloid Abeta into off-pathway conformers, J. Biol. Chem. 285 (2010) 24228–24237, https://doi.org/10.1074/jbc.M110.133108.
[63] K. Ono, L. Li, Y. Takamura, Y. Yoshiike, L. Zhu, F. Han, X. Mao, T. Ikeda, J. Takasaki, H. Nishijo, A. Takashima, D.B. Teplow, M.G. Zagorski, M. Yamada, Phenolic compounds prevent amyloid β-protein oligomerization and synaptic dysfunction by site-specific binding, J. Biol. Chem. 287 (2012) 14631–14643, https://doi.org/10.1074/jbc.M111.325456.
[64] Q. Zhang, X. Hu, W. Wang, Z. Yuan, Study of a bifunctional Aβ aggregation inhibitor with the abilities of antiamyloid-β and copper chelation, Biomacromolecules 17 (2016) 661–668, https://doi.org/10.1021/acs.biomac.5b01603.
[65] F. Boscia, A. Pannaccione, R. Ciccone, A. Casamassa, C. Franco, I. Piccialli, V. de Rosa, A. Vinciguerra, G. Di Renzo, L. Annunziato, The expression and activity of K_V3.4 channel subunits are precociously upregulated in astrocytes exposed to Aβ oligomers and in astrocytes of Alzheimer's disease Tg2576 mice, Neurobiol. Aging 54 (2017) 187–198, https://doi.org/10.1016/j.neurobiolaging.2017.03.008.
[66] C.A. McLean, R.A. Cherny, F.W. Fraser, S.J. Fuller, M.J. Smith, K. Beyreuther, A. I. Bush, C.L. Masters, Soluble pool of Abeta amyloid as a determinant of severity of neurodegeneration in Alzheimer's disease, Ann. Neurol. 46 (1999) 860–866, https://doi.org/10.1002/1531-8249(199912)46:6<860::aid-ana8>3.0.co;2-m.
[67] N.J. Izzo, A. Staniszewski, To.L. Fa, M. Teich, A.F. Saeed, F. Wostein, H. Walko, T. Vaswani 3rd, A. Wardius, M. Syed, Z. Ravenscroft, J. Mozzoni, K. Silky, C. Rehak, C. Yurko, R. Finn, P. Look, G. Rishton, G. Safferstein, H. Miller,

M. Johanson, C. Stopa, E. Windisch, M. Hutter-Paier, B. Shamloo, M. Arancio, O. LeVine H 3rd, Catalano SM. Alzheimer's therapeutics targeting amyloid beta 1-42 oligomers I: Abeta 42 oligomer binding to specific neuronal receptors is displaced by drug candidates that improve cognitive deficits, PLoS One 9 (2014), e111898, https://doi.org/10.1371/journal.pone.0111898.

[68] D. Krishnan, R.N. Menon, P.S. Mathuranath, S. Gopala, A novel role for SHARPIN in amyloid-β phagocytosis and inflammation by peripheral blood-derived macrophages in Alzheimer's disease, Neurobiol. Aging 93 (2020) 131–141, https://doi.org/10.1016/j.neurobiolaging.2020.02.001. Epub 2020 Feb 13.

[69] Y. Luo, S. Zhou, H. Haeiwa, R. Takeda, K. Okazaki, M. Sekita, T. Yamamoto, M. Yamano, K. Sakamoto, Role of amber extract in protecting SHSY5Y cells against amyloid β1-42-induced neurotoxicity, Biomed. Pharmacother. 141 (2021), 111804, https://doi.org/10.1016/j.biopha.2021.111804.

[70] F. Amar, M.A. Sherman, T. Rush, M. Larson, G. Boyle, L. Chang, J. Götz, A. Buisson, S.E. Lesné, The amyloid-β oligomer Aβ*56 induces specific alterations in neuronal signaling that lead to tau phosphorylation and aggregation, Sci. Signal 10 (2017) eaal2021, https://doi.org/10.1126/scisignal.aal2021.

[71] H.L. Nguyen, H.Q. Linh, P. Krupa, G. La Penna, M.S. Li, Amyloid β dodecamer disrupts the neuronal membrane more strongly than the mature fibril: understanding the role of oligomers in neurotoxicity, J. Phys. Chem. B. 126 (2022) 3659–3672, https://doi.org/10.1021/acs.jpcb.2c01769.

[72] F. Bisceglia, A. Natalello, M.M. Serafini, R. Colombo, L. Verga, C. Lanni, E. De Lorenzi, An integrated strategy to correlate aggregation state, structure and toxicity of Aß 1-42 oligomers, Talanta 188 (2018) 17–26, https://doi.org/10.1016/j.talanta.2018.05.062.

[73] H.A. Scheidt, I. Morgado, S. Rothemund, D. Huster, M. Fändrich, N.M.R. Solid-state, spectroscopic investigation of Aβ protofibrils: implication of a β-sheet remodeling upon maturation into terminal amyloid fibrils, Angew. Chem. Int. Ed. Engl. 50 (2011) 2837–2840, https://doi.org/10.1002/anie.201007265.

[74] Micsonai A., Wien F., Kernya L., Lee Y.H., Goto Y., Réfrégiers M., Kardos J. Accurate secondary structure prediction and fold recognition for circular dichroism spectroscopy. Proc. Natl. Acad. Sci. U. S. A. 112 (2015) E3095–3103. doi: 10.1073/pnas.1500851112.

[75] D. Marasco, C. Vicidomini, P. Krupa, F. Cioffi, P.D.Q. Huy, M.S. Li, D. Florio, K. Broersen, M.F. De Pandis, G.N. Roviello, Plant isoquinoline alkaloids as potential neurodrugs: a comparative study of the effects of benzo[c] phenanthridine and berberine-based compounds on β-amyloid aggregation, Chem. Biol. Interact. 334 (2021), 109300, https://doi.org/10.1016/j.cbi.2020.109300.

[76] M.D. Kirkitadze, M.M. Condron, D.B. Teplow, Identification and characterization of key kinetic intermediates in amyloid beta-protein fibrillogenesis, J. Mol. Biol. 312 (2001) 1103–1119, https://doi.org/10.1006/jmbi.2001.4970.

[77] O. Crescenzi, S. Tomaselli, R. Guerrini, S. Salvadori, A.M. D'Ursi, P.A. Temussi, D. Picone, Solution structure of the Alzheimer amyloid beta-peptide (1-42) in an apolar microenvironment. Similarity with a virus fusion domain, Eur. J. Biochem. 269 (2002) 5642–5648, https://doi.org/10.1046/j.1432-1033.2002.03271.x.

[78] S. Shuaib, B. Goyal, Scrutiny of the mechanism of small molecule inhibitor preventing conformational transition of amyloid-β_{42} monomer: insights from molecular dynamics simulations, J. Biomol. Struct. Dyn. 36 (2018) 663–678, https://doi.org/10.1080/07391102.2017.1291363.

[79] J.W.D. Griffin, P.C. Bradshaw, Residue interaction network analysis predicts a Val24-Ile31 interaction may be involved in preventing amyloid-beta (1-42) primary nucleation, Protein J. 40 (2021) 175–183, https://doi.org/10.1007/s10930-021-09965-w.

[80] Lührs T., Ritter C., Adrian M., Riek-Loher D., Bohrmann B., Döbeli H., Schubert D., Riek R. 3D structure of Alzheimer's amyloid-beta(1–42) fibrils. Proc. Natl. Acad. Sci. U. S. A. 102 (2005) 17342–17347. doi: 10.1073/pnas.0506723102.

[81] T. Sato, P. Kienlen-Campard, M. Ahmed, W. Liu, H. Li, J.I. Elliott, S. Aimoto, S. N. Constantinescu, J.N. Octave, S.O. Smith, Inhibitors of amyloid toxicity based on beta-sheet packing of Abeta40 and Abeta42, Biochemistry 45 (2006) 5503–5516, https://doi.org/10.1021/bi052485f.

[82] S.S. Barale, R.S. Parulekar, P.M. Fandilolu, M.J. Dhanavade, K.D. Sonawane, Molecular insights into destabilization of Alzheimer's Aβ protofibril by arginine containing short peptides: a molecular modeling approach, ACS Omega 4 (2019) 892–903, https://doi.org/10.1021/acsomega.8b02672.

[83] P.K. Kanchi, A.K. Dasmahapatra, Destabilization of the Alzheimer's amyloid-β protofibrils by THC: a molecular dynamics simulation study, J. Mol. Graph. Model 105 (2021), 107889, https://doi.org/10.1016/j.jmgm.2021.107889.

[84] M.S. Dutta, S. Basu, Identifying the key residues instrumental in imparting stability to amyloid beta protofibrils - a comparative study using MD simulations of 17-42 residues, J. Biomol. Struct. Dyn. 39 (2021) 431–456, https://doi.org/10.1080/07391102.2019.1711192.

[85] R.J. Chalifour, R.W. McLaughlin, L. Lavoie, C. Morissette, N. Tremblay, M. Boulé, P. Sarazin, D. Stéa, D. Lacombe, P. Tremblay, F. Gervais, Stereoselective interactions of peptide inhibitors with the beta-amyloid peptide, J. Biol. Chem. 278 (2003) 34874–34881, https://doi.org/10.1074/jbc.M212694200.

[86] A. Rauk, The chemistry of Alzheimer's disease, Chem. Soc. Rev. 38 (2009) 2698–2715, https://doi.org/10.1039/b807980n.

[87] M. Ahmed, J. Davis, D. Aucoin, T. Sato, S. Ahuja, S. Aimoto, J.I. Elliott, W.E. Van Nostrand, S.O. Smith, Structural conversion of neurotoxic amyloid-beta(1-42) oligomers to fibrils, Nat. Struct. Mol. Biol. 17 (2010) 561–567, https://doi.org/10.1038/nsmb.1799.

[88] J. Adler, M. Baumann, B. Voigt, H.A. Scheidt, D. Bhowmik, T. Häupl, B. Abel, P. K. Madhu, J. Balbach, S. Maiti, D. Huster, A detailed analysis of the morphology of fibrils of selectively mutated amyloid β (1-40), Chemphyschem 17 (2016) 2744–2753, https://doi.org/10.1002/cphc.201600413.

[89] F. Hoffmann, J. Adler, B. Chandra, K.R. Mote, G. Bekçioğlu-Neff, D. Sebastiani, D. Huster, Perturbation of the F19-L34 contact in amyloid β (1-40) fibrils induces only local structural changes but abolishes cytotoxicity, J. Phys. Chem. Lett. 8 (2017) 4740–4745, https://doi.org/10.1021/acs.jpclett.7b02317.

[90] A.K. Das, A. Rawat, D. Bhowmik, R. Pandit, D. Huster, S. Maiti, An early folding contact between Phe19 and Leu34 is critical for amyloid-β oligomer toxicity, ACS Chem. Neurosci. 6 (2015) 1290–1295, https://doi.org/10.1021/acschemneuro.5b00074.

[91] A. Korn, D. Surendran, M. Krueger, S. Maiti, D. Huster, Ring structure modifications of phenylalanine 19 increase fibrillation kinetics and reduce toxicity of amyloid β (1-40), Chem. Commun. 54 (2018) 5430–5433, https://doi.org/10.1039/c8cc01733f.

[92] P.P. Rao, T. Mohamed, W. Osman, Investigating the binding interactions of galantamine with β-amyloid peptide, Bioorg. Med. Chem. Lett. 23 (2013) 239–243, https://doi.org/10.1016/j.bmcl.2012.10.111.

[93] S. Chakraborty, S. Basu, Insight into the anti-amyloidogenic activity of polyphenols and its application in virtual screening of phytochemical database, Med. Chem. Res. 23 (2014) 5141–5148, https://doi.org/10.1007/s00044-014-1081-2.

[94] A. Pannaccione, I. Piccialli, A. Secondo, R. Ciccone, P. Molinaro, F. Boscia, L. Annunziato, The Na^+/Ca^{2+} exchanger in Alzheimer's disease, Cell Calcium 87 (2020), 102190, https://doi.org/10.1016/j.ceca.2020.102190.

[95] S. Chakroborty, G.E. Stutzmann, Early calcium dysregulation in Alzheimer's disease: setting the stage for synaptic dysfunction, Sci. China Life Sci. 54 (2011) 752–762, https://doi.org/10.1007/s11427-011-4205-7.

[96] A. Demuro, E. Mina, R. Kayed, S.C. Milton, I. Parker, C.G. Glabe, Calcium dysregulation and membrane disruption as a ubiquitous neurotoxic mechanism of soluble amyloid oligomers, J. Biol. Chem. 280 (2005) 17294–17300, https://doi.org/10.1074/jbc.M500997200.

[97] A. Demuro, I. Parker, "Optical patch-clamping": single-channel recording by imaging Ca2+ flux through individual muscle acetylcholine receptor channels, J. Gen. Physiol. 126 (2005) 179–192, https://doi.org/10.1085/jgp.200509331.

[98] R. Resende, E. Ferreiro, C. Pereira, C. Resende de Oliveira, Neurotoxic effect of oligomeric and fibrillar species of amyloid-beta peptide 1-42: involvement of endoplasmic reticulum calcium release in oligomer-induced cell death, Neuroscience 155 (2008) 725–737, https://doi.org/10.1016/j.neuroscience.2008.06.036.

[99] E. Alberdi, M.V. Sánchez-Gómez, F. Cavaliere, A. Pérez-Samartín, J.L. Zugaza, R. Trullas, M. Domercq, C. Matute, Amyloid beta oligomers induce Ca2+ dysregulation and neuronal death through activation of ionotropic glutamate receptors, Cell Calcium 47 (2010) 264–272, https://doi.org/10.1016/j.ceca.2009.12.010.

[100] E.C. Toescu, A. Verkhratsky, The importance of being subtle: small changes in calcium homeostasis control cognitive decline in normal aging, Aging Cell 6 (2007) 267–273, https://doi.org/10.1111/j.1474-9726.2007.00296.x.

[101] E. Pchitskaya, E. Popugaeva, I. Bezprozvanny, Calcium signaling and molecular mechanisms underlying neurodegenerative diseases, Cell Calcium 70 (2018) 87–94, https://doi.org/10.1016/j.ceca.2017.06.008.

[102] B.L. Kagan, J. Thundimadathil, Amyloid peptide pores and the beta sheet conformation, Adv. Exp. Med. Biol. 677 (2010) 150–167, https://doi.org/10.1007/978-1-4419-6327-7_13.

[103] J.H. Viles, Imaging amyloid-β membrane interactions: ion-channel pores and lipid-bilayer permeability in Alzheimer's disease, Angew. Chem. Int. Ed. Engl. 62 (2023), e202215785, https://doi.org/10.1002/anie.202215785.

[104] H. Jang, F.T. Arce, S. Ramachandran, R. Capone, R. Azimova, B.L. Kagan, R. Nussinov, R. Lal, Truncated beta-amyloid peptide channels provide an alternative mechanism for Alzheimer's disease and Down syndrome, Proc. Natl. Acad. Sci. U. S. A. 107 (2010) 6538–6543, https://doi.org/10.1073/pnas.0914251107.

[105] R. Capone, H. Jang, S.A. Kotler, B.L. Kagan, R. Nussinov, R. Lal, Probing structural features of Alzheimer's amyloid-β pores in bilayers using site-specific amino acid substitutions, Biochemistry 51 (2012) 776–785, https://doi.org/10.1021/bi2017427.

[106] D.A. Butterfield, Amyloid beta-peptide (1-42)-induced oxidative stress and neurotoxicity: implications for neurodegeneration in Alzheimer's disease brain. A review, Free. Radic. Res. 36 (2002) 1307–1313, https://doi.org/10.1080/1071576021000049890.

[107] D.A. Butterfield, D. Boyd-Kimball, Oxidative stress, amyloid-β peptide, and altered key molecular pathways in the pathogenesis and progression of Alzheimer's disease, J. Alzheimers Dis. 62 (2018) 1345–1367, https://doi.org/10.3233/JAD-170543.

[108] S. Jin, N. Kedia, E. Illes-Toth, I. Haralampiev, S. Prisner, A. Herrmann, E. E. Wanker, J. Bieschke, Amyloid-β(1-42) aggregation initiates its cellular uptake and cytotoxicity, J. Biol. Chem. 291 (2016) 19590–19606, https://doi.org/10.1074/jbc.M115.691840.

[109] M.G. Iadanza, M.P. Jackson, E.W. Hewitt, N.A. Ranson, S.E. Radford, A new era for understanding amyloid structures and disease, Nat. Rev. Mol. Cell Biol. 19 (2018) 755–773, https://doi.org/10.1038/s41580-018-0060-8.

[110] B. Guivernau, J. Bonet, V. Valls-Comamala, M. Bosch-Morató, J.A. Godoy, N. C. Inestrosa, A. Perálvarez-Marín, X. Fernández-Busquets, D. Andreu, B. Oliva, F. J. Muñoz, Amyloid-β peptide nitrotyrosination stabilizes oligomers and enhances NMDAR-mediated toxicity, J. Neurosci. 36 (2016) 11693–11703, https://doi.org/10.1523/JNEUROSCI.1081-16.2016.

[111] M. Sakono, T. Zako, Amyloid oligomers: formation and toxicity of Abeta oligomers, FEBS J. 277 (2010) 1348–1358.